Air Force Institute of Technology

AFIT Scholar

Theses and Dissertations

Student Graduate Works

3-22-2012

Computer Aided Multi-Data Fusion Dismount Modeling

Juan L. Morales

Follow this and additional works at: https://scholar.afit.edu/etd

Part of the Electrical and Computer Engineering Commons, and the Statistics and Probability Commons

COMPUTER AIDED MULTI-DATA FUSION DISMOUNT MODELING

THESIS

Juan L. Morales, Captain, USAF

AFIT/GE/ENG/12-29

DEPARTMENT OF THE AIR FORCE
AIR UNIVERSITY

AIR FORCE INSTITUTE OF TECHNOLOGY

Wright-Patterson Air Force Base, Ohio

APPROVED FOR PUBLIC RELEASE; DISTRIBUTION UNLIMITED

AFIT/GE/ENG/12-29

COMPUTER AIDED MULTI-DATA FUSION DISMOUNT MODELING

THESIS

Presented to the Faculty

Department of Electrical and Computer Engineering

Graduate School of Engineering and Management

Air Force Insitute of Technology

Air University

Air Education and Training Command

in Partial Fulfillment of the Requirements for the

Degree of Master of Science in Electrical Engineering

Juan L. Morales, B.S.E.E., M.B.A., P.E.
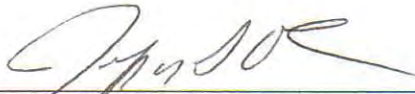
Captain, USAF

March 2012

AFIT/GE/ENG/12-29

COMPUTER AIDED MULTI-DATA FUSION DISMOUNT MODELING

Juan L. Morales, B.S.E.E., M.B.A., P.E.
Captain, USAF

Approved:

_____
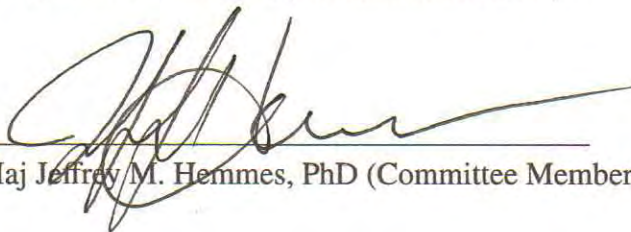Lt.Col. Jeffrey D. Clark, PhD (Chairman)

27 Feb 12
Date

_____
Dr. Gilbert L. Peterson, (Committee Member)

27 FEB 2012
Date

_____
Maj Jeffrey M. Hemmes, PhD (Committee Member)

27 Feb 2012
Date

Abstract

Recent research efforts strive to address the growing need for dismount surveillance, dismount tracking and characterization. Current work in this area utilizes hyperspectral and multispectral imaging systems to exploit spectral properties in order to detect areas of exposed skin and clothing characteristics. Because of the large bandwidth and high resolution, hyperspectral imaging systems pose great ability to characterize and detect dismounts. The acquisition and modification of hyperspectral images presents several challenges and inconveniences for researchers. They are dependent on a particular environmental condition. They are costly, cumbersome, and involve dedicated software practices and particular knowledge to operate. A simple system where the development and enhancement of multi-data dismount models becomes a grand necessity. This thesis demonstrates a computer aided multi-data fused dismount model, for greater ease of dismount detection, characterization and identification. The system is created by fusing: pixel mapping, signature attachment, and pixel mixing algorithms.

The developed multi-data dismount model produces simulated hyperspectral images that closely represents an image collected by a hyperspectral imager. The dismount model can be modified to fit the researcher's needs. The multi-data model structure allows the employment of a database of signatures acquired from several sources (i.e., Spectroradiometer, or hyperspectral imagers). The model is flexible enough to allow further exploitation, enhancement and manipulation. For example, the addition of facial details, addition of background objects, dismount skin signatures, clothing signatures, modification to the position, pose, size, and appearance of the dismount and more. The multi-data dismount model developed in this effort fulfills the need for a dismount modeling tool in a hyperspectral imaging environment.

Acknowledgments

I would like to give thanks to all of the professors with whom I had the benefit of having a class, especially to Maj Hemmes and Dr. Peterson for being part of my thesis committee, taking the time to review my thesis work and for those challenging courses they offer. I would also like to thank LtCol Clark for being a great advisor and for all the help and guidance he provided. This is much appreciated and was indispensable to achieving this goal.

Thanks also go to fellow students whose support was invaluable. Also, many thanks to the USAF and this great Nation for giving me the privilege of work and sustain my family.

I'll like to give countless thanks to my beautiful wife and children for love, understanding and support. Finally, but most importantly, I'll like to offer many thanks and praise to God, for allowing me to be here, having mercy and helping me all the way.

<div align="center">Juan L. Morales</div>

Table of Contents

List of Figures

x

List of Tables

List of Abbreviations

COMPUTER AIDED MULTI-DATA FUSION DISMOUNT MODELING

1   Introduction

United States Armed Forces and Law Enforcement communities continue to stress the importance of research into persistent surveillance capabilities that provide detection and characterization of dismounts. The United States Air Force (USAF) in Doctrine Document 1 (AFDD-1) states that "As a leader in military application of air, space, and intelligence, surveillance, and reconnaissance technology, the Air Force is committed to innovation to guide research, development, and fielding of unsurpassed capabilities" [3].

Due to the general shift from conventional warfare to terrorism and urban warfare, locating and tracking individuals of interest has become of vital importance [3]. Recent research efforts address this growing need for dismount surveillance, as well as dismount tracking and characterization. These research efforts include,

1. Defense Advance Research Project Agency (DARPA) Combat Zones that See program (CTS) [2], which has the goal of creating networks of cameras and sensors to monitor everything that moves and report observations to an operation center.

2. United States Army research effort towards the development of algorithms for the Unmanned Air Vehicle (UAV) ISR system, with the objective of tracking targets in urban and others environments [6].

The conception of a model to simulate dismounts, as well as the scene background, is necessary. Therefore the thesis, combine several dismount characteristics, clothing and environmental signatures, dismount detection and characterization, in a multi-data modeling environment to create a dismount model.

1.1 Problem Statement

Recent research efforts [12, 16, 29, 15] have provided the ability to detect dismounts (humans) from the background in different environment conditions. In [12], a robust method for dismount detection is proposed, based on skin detection using near-infrared wavelengths. Several different techniques previously studied on dismount characterization and detection include, hyperspectral skin detection [12, 16], blinking detection, movement detection, face detection and recognition [37], and red-green-blue (RGB) skin characterization.

The goal of this thesis is to create and demonstrate the feasibility of a systematic method to construct a multi-data fused dismount model for the demanding studies of detection, characterization and identification. The techniques of our dismount representation include current studies in skin detection, face detection, and skin and clothing characterization. The integration of these approaches are used to render an dismount model. Using the multi-data dismount model, an operator or an algorithm will recognize, characterize, and identify distinctive features of specific individuals for use in classification and characterization. Furthermore, the system should provide a platform capable of supplementary expansion for the later integration of new capabilities for dismount modeling.

1.2 Scope

Limitations of this project include the availability of hyperspectral images containing several individuals of different ethnicity, pose positions and clothing arrangements. In order to achieve our objective, the tasks accomplished by this research effort are the following:

1. Explore methods for dismount representation and data-fused modeling.

2. Analyze image acquisition technologies used to detect dismounts and skin (hyperspectral, multispectral and Red-Green-Blue).

3. Research and study different dismount detection techniques and their capabilities with the objective of meeting information requirements for such techniques.

4. Research the approaches towards dismount characterization and identification.

5. Develop a fusion based computer aided multi-data dismount model.

6. Acquire hyperspectral signatures, i.e. skin tones, backgrounds, dismount shape/contours, and clothing.

7. Integrate the previous tasks to create a modeled scene.

8. Integrate sub-pixel mixing for final scene rendering.

The result is a computer aided dismount model that provides the basis for a complete and accurate dismount modeling research tool. The use of the system can grow the potential of generating improvements on characterization of individuals by an efficient, easy to acquire, quick to develop, robust human modeling design.

1.3 Document Organization

Chapter II provides a discussion of research literature related to human modeling. This chapter also contains the background information on several approaches for human characterization, different types of multi-data signatures to be used in the model, pixel mixing and finally a basic edge detection algorithm.

Chapter III presents the methodology by describing the systematic creation of the data-fused dismount model. It describes the architecture of the system and explains in details the steps for the creation of the multi-data dismount model. This chapter also provides details of the possible configurations for the dismount and scene model.

The experimental results and analysis are provided in chapter IV. This includes the validation of functionality and design of the dismount model, integrating several hyperspectral signatures from different sources. Chapter IV also compares the resemblance of the computer aided dismount model versus a hyperspectral picture from a camera and gives advantages and disadvantages of the proposed dismount model.

Chapter V summarizes the results, and discusses the impact of this thesis on dismount modeling towards the studies of characterization and identification, and provides recommendations for future work in enhancing dismount modeling.

2 Background

An overview of some prominent approaches for dismount modeling, as well as, the necessary background information on imaging spectroscopy for multi-data fusion and its function for sub-pixel mixing is discussed in this chapter.

Section 2.1 introduces several approaches for dismount modeling. These include morphological models and topological models. Section 2.3 introduces imaging spectroscopy and the approaches towards dismount and scene representation in an image. Finally, Section 2.4 describes methods for sub-pixel mixing with the objective of mimicking realistic dismount representation.

2.1 Dismount Modeling

There are two primary dismount representations are: physiology, and behavioral [9]. The physiological representation refers to shape or geometry of the dismount [33]. A behavioral representation is related to gait (manner of walking), voice sounds, or individual proceedings [9]. For the purpose of this thesis, the focus is on the human ontology representation that specifically encompasses the visual physiology of a dismount.

Ontology is a formal representation of knowledge as a set of concepts within a domain and the relationship between those concepts [38]. An ontological representation of a dismount is closely linked to the graphical representation. It is necessary to switch from the graphical representation to the ontology representation and vice versa. This is possible due to the use of human shape descriptors like landmarks, body composition, body segmentation, skeletonisation, body representation using geometrical shapes, and the relation between them.

Abstract forms of dismount modeling (computer aided dismount modeling) are necessary to study dismount ontological representations. These concepts are based on human morphological and topological models.

2.1.1 Morphological Models. Morphology is a branch of bioscience dealing with the study of the form and structure of organisms and their specific structural features [19]. This includes aspects of the outward appearance (shape, structure, color, pattern).

The analysis of the dismount shape aims to extract features such as body landmarks, skeletal structure and body composition. These features serve for human representation and modeling purposes.

2.1.1.1 Body Landmarks Methods. In the Fig. 2.1 and Fig. 2.2 it is demonstrated how the author of [39] applied fuzzy logic to extract landmark features (armhole, neck, chest, crotch and belly button) from three dimensional (3D) body scans. This approach uses landmark extraction based on an analysis of the human shape.
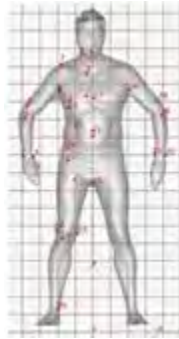
Figure 2.1: Human body morphological landmarks [39].

There are three recognized categories of dismounts body landmarks [30]:

1. Locally defined landmarks, defined in terms of structures close to a point; for example, an intersection between three structures.

2. The intermediate landmarks, includes points such as the edge of the structure, or local minima and maxima of a curvature. They are defined in terms of local features, but they are not surrounded on all sides like the first type.

6
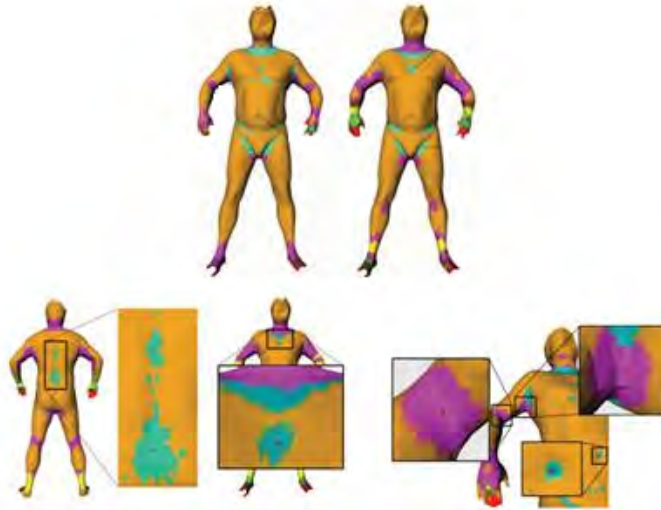
Figure 2.2: Samples of landmark feature extraction from body scans (arm hole, neck, chest, crotch and belly button) [39].

3. Points far away from the landmark, which are commonly defined in terms of a point "furthest away" from another point is the last landmark.

In addition to landmarks, there are "semi-landmarks", which are points along a curve. Their position along the curve is arbitrary but these points provide information about the curvature in multiple dimensions.

In order to compare different dismount models, using landmark extraction, *shape analysis* must be accomplished. By definition, shape is not altered by translation, scale or rotation [25]. Therefore, to compare shapes, the non-shape information is removed from the landmark coordinates. In one step, the shapes are translated (the same two coordinates are fixed to those values), scaled (to unit baseline length) and rotated as explained in [10].

An alternative, and preferred method, is *procrustes superimposition*. This method translates the center of the shapes to (0, 0). The 'x' center of the centroid is the average of the x-coordinates of the landmarks of an individual. The 'y' coordinate of the centroid is the average of the y-coordinates. Shapes are scaled to unit centroid size, which is the square root of the summed squared distances of each landmark to the centroid. The

7

configuration is rotated to minimize the deviation between it and a reference, typically the mean shape. In the case of semi-landmarks, variation in position along the curve is also removed. For the case of curved semi-landmarks shape space, analysis is accomplished by projecting shapes onto a space tangent to the shape space. Within the tangent space, conventional multivariate statistical methods, such as multivariate analysis of variance and multivariate regression, can be used to test statistical hypotheses about the shape.

Researches have discovered that this method of procrustes-based analysis has some limitations as mentioned in [31, 38].

1. The procrustes superimposition uses a least-squares criterion to find the optimal rotation. This variation is localized to a single landmark and transferred out. This is called the "Pinocchio Effect."

2. The superimposition may impose a pattern of covariation on the landmarks.

3. Features that are not captured by landmarks and semi-landmarks cannot be analyzed. Moreover, there are criticisms of procrustes-based methods that motivate an alternative approach to analyzing landmark data.

It is mentioned in [37] that the computational methods involved in the extraction of features, such as landmarks or shape segmentation, must comply with two main constraints:

1. Landmark extraction and morphological segmentation results must be anthropometrically consistent.

2. Landmark extraction and morphological segmentation results must be consistent and almost invariant from one data set to another.

The method of landmark based-modeling may be useful for dismount representation. Although, based on the constraints described above, it is concluded that the use of

dismount landmark features with the purpose of characterization, may present a challenge in regards to data acquisition and computational analysis. Also, when considering the field of computer vision, it has been demonstrated that this approach is highly dependent on the landmark feature detection algorithm. A minimum discrepancy in correctly identifying a landmark position size or shape, or a landmark parse, will present a problem for an accurate representation.

       2.1.1.2   Body Outline Method.   According to [8], pertinent information about an object is often contained in the shape of its boundaries. Experiments have demonstrated that human vision is capable of recognizing an object by the shape of its boundaries alone. For example, Fig. 2.3 shows a human body outline. This recognition approach is implemented in [8] using the Hough Transform.

    Outline analysis is another approach to analyzing shape. Outline analysis is distinguished from other approaches by the use of coefficients of mathematical functions that are fitted to points sampled along the outline. Older techniques such as the "fit to a polynomial curve" [22] and principal components quantitative analysis [39], have been superseded by the eigen-shape analysis [19], and elliptical Fourier analysis [25] approaches. Eigen-shape analysis [28] involves fitting a preset number of semi-landmarks at equal intervals around the outline of a shape. This is shown in [10] by recording the deviation of each angle from one semi-landmark to another semi-landmark of a simple circle. Elliptical Fourier analysis defines the outline as the sum of the minimum number of ellipses required to mimic the shape [31].

    Body outline methods have their weaknesses; the most dangerous (and easily overcome) is their susceptibility to noise in the outline [38]. Likewise, neither compares homologous points, and global change carries more weight than local variation (which may have large consequences in regards to human representation).

Figure 2.3: Representative outline of the human body, it is used to calculate and analyze human body shape [7].

Eigen-shape analysis [28] requires an equivalent starting point to be set for each specimen, which can be a source of error. Elliptical Fourier analysis [25] also suffers from redundancy in that not all variables are independent [38]. On the other hand, it is possible to apply both techniques to complex curves without having to define a centroid. This makes removing the effect of location, size and rotation much simpler as explained in [38].

The perceived failings of the body outline method is that points of a homologous origin are not compared, and it oversimplifies complex shapes by considering only the outline and not internal changes. Ballard [8] identified that the approximation of the body outline as a shortcoming, hence it deals poorly with pointed shapes.

Another criticism of the body outline-based methods is that they ignore homology. A famous example of this problem is that it mistakes a scapula for a potato chip [24]. Such a comparison would not be possible if the data were restricted to biologically homologous points.

2.1.1.3   Skeletal Essence and Body Composition.   Anatomical features, i.e. skeletal structure, is the basis of another type of dismount representation. The skeleton of a body is the locus of the center of all its interior maximal circles (2D) or spheres (3D) [14] (Fig. 2.4). Together with the associated radius function, which is the radius of the maximal ball around any given point on the skeleton, the object can be represented with

less information than the object itself. Such a technique can be applied in human shape representation (or description). Commonly, skeletal representations can be derived by:

1. Computing a distance transform that yields the shortest distance from each interior point of a region to its border or,

2. By identifying at each point the largest possible size of the primitive shape such that it is entirely contained in a region to be represented.

The skeletal representation is derived by identifying the primitives having locally maximal sizes. These approaches are straightforward, but computationally costly since the distance computation must be performed at every point.

The authors in [14] present a concept of obtaining the skeleton of 3-D polyhedral regions in a computationally efficient manner. The efficiency of the approach results from the use of an intermediate, analog representation of the given shape information, which is called the potential field. Potential field representation avoids the expensive task of computing the distance transform at each pixel. The computation is limited to the locations of the locally maximal primitives.

The computation of the potential field can be performed efficiently if the shape information is given in a compact form, i.e. the polyhedral representation of the surface. This compact description may be directly available as a part of the specification of the given object shape or it may be derived from the given object data such as its surface or volume descriptions.

The international standard anatomical position is the position that provides a reference point for describing the individual structures of the human body. In this position, the body is standing erect with good posture and the face is looking directly forward in a normal manner. The feet are close together, flat on the floor and the toes pointing forward. The arms are down at the sides with the palms turned forward. It is
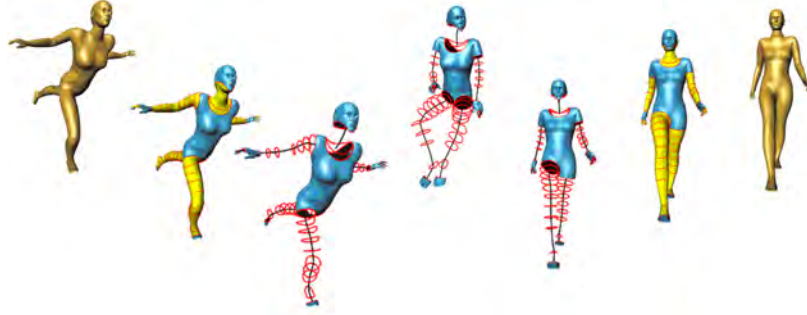
Figure 2.4: Polyhedral representation using skeletal essence and body composition [4].

necessary for all of the individuals to be in this position in order to correctly approximate skeletal structure and body composition [29]. Therefore, to effectively use this approach as comparison the position needs to be standard and universal between every sample.

In conclusion, the use of anatomical characteristics for human representation presents several constraints as mentioned above. The position, location and points of reference need to be standard between all of the samples. Computational limitations may take place (depending on the technique) and the method is highly dependent on edge detection algorithms.

2.1.2 Topological Model. Topology-based modeling approach utilize 3-D point clouds [29] or topological structures of 3-D models [24] as shown in Fig. 2.5 to measure the similarity between different human bodies or objects.

The difficulties of the topology-based approach include automatic topology extraction from all types of 3-D models, and the discrimination between topologies from different individuals. The authors in [24] propose a novel method called Topology Matching where the similarity between polyhedral models are quickly, accurately, and automatically calculated by comparing Multiresolutional Reeb Graphs (MRG).

The MRG [24] represents the topological structure of a 3-D shape at various levels of resolution. The MRG is created using a continuous function on the 3-D shape, which may

12

preferably be a function of geodesic distance. This function is invariant to rotation or translation and is also good against variations in connectivity caused by a mesh simplification or subdivision. The similarity between 3-D shapes is calculated using a coarse-to-fine strategy while preserving the consistency of the graph structures, which results in establishing a correspondence between the parts of objects. According to the author, the similarity calculations of this approach is fast and efficient. It is not necessary to determine the particular pose of a 3-D shape, such as a rotation, in advance.

Experiments conducted in [24] indicate that Topology Matching provides a fast and efficient computation of the similarity and correspondence between shapes and provides results that agree well with human intuition.
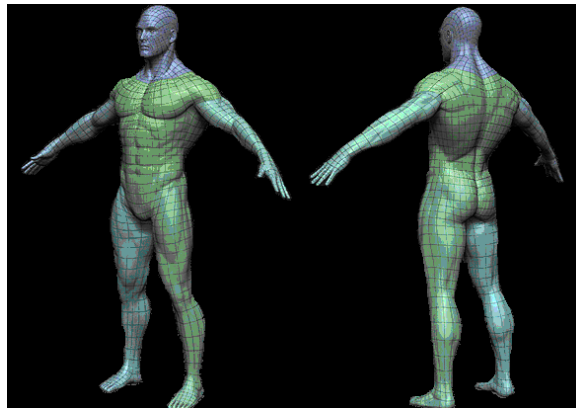
Figure 2.5: Human topological representation [41].

One advantage for a topology-based approach in regards to dismount representation is that it leads to highly similar characteristics between two identical 3-D models with different gestures or poses, which is not able to be effectively accomplished using shape-based methods. However, shape-based approaches result in a high similarity between 3-D models with different connections among parts, whereas a topology-based approach cannot do the same. This is illustrated by considering that fingers and a shoulder of a dismount model are both parts of a human body. However, the topologies are quite

13

different whether the finger does or does not connect to a human body, yet finger shapes are similar [24].

2.2 Digital Imaging and Remote Sensing Image Generation

The Digital Imaging and Remote Sensing Image Generation (DIRSIG) model is a synthetic image generation model engineered by the Digital Imaging and Remote Sensing Laboratory at Rochester Institute of Technology [36]. The model can produce multispectral or hyperspectral imagery from the visible through the thermal infrared region of the electromagnetic spectrum, which is the same capability of the proposed model in this thesis.

The model developed by DIRSIG, as well as the thesis proposed model, can be used to test image system designs, to create test imagery for evaluating image exploitation algorithms and for creating data for training image analysts. The approach for this thesis differs from DIRSIG in basic concept. This thesis focuses on modeling dismounts in a scene, where DIRSIG focuses on scene modeling and currently does not incorporate dismounts.

2.3 Imaging Spectroscopy

Many different types of image data can be used to represent dismounts. The most common systems employs visible range parameters, near-infrared, far infrared, or some combination of these (Fig. 2.6).

2.3.1 Visual Spectra Images. Common standard color cameras take images at three different wavelengths of light, corresponding to red, green and blue (RGB). The visible region of the electromagnetic spectrum is frequently used to depict dismounts due to the accessibility and low acquisition costs. Monochrome (gray-scale) and RGB cameras are commonly used in this matter. For example, dismount representation using

14
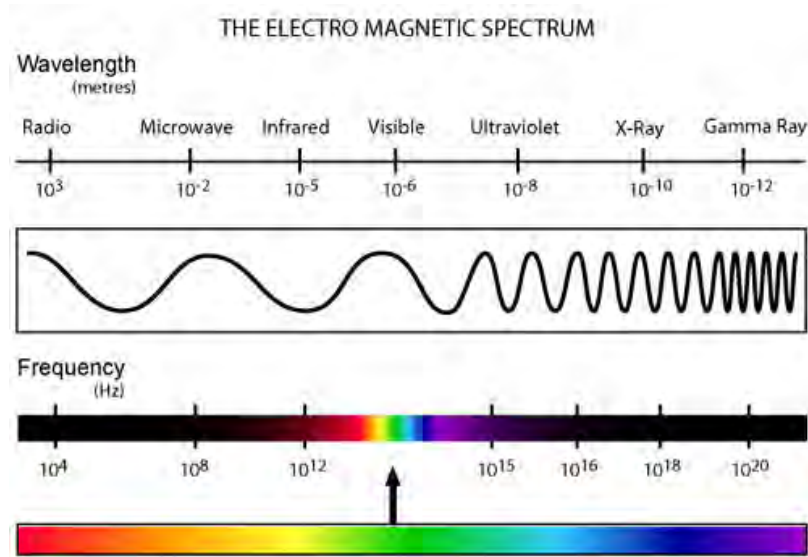
Figure 2.6: Electromagnetic Spectrum. Hyperspectral images use near-infrared, far-infrared and visible segments of the Electro Magnetic Spectrum [1].

RGB and gray-scale can be found in dismount detection [32, 18], and face recognition [37]. It has been found that these approaches are effective in limited conditions and further development is necessary for a robust dismount detection, recognition and characterization.

2.3.2 Far-Infrared Images. An alternative to the visible region dismount representation is to acquire an image with the far-infrared spectrum. This technique has several prominent benefits for the remote sensing community and dismount characterization [20]. This type of remote sensing is strongly characterized by thermal emissions. Consequently, dismounts appear brighter than the background and tend to stand out well. Additionally, image factors such as lighting, color, texture, and shadowing that would normally disrupt exposure in visual light images have less of an impact in the infrared range.

However infrared imagery does have its own limitations. Many objects including animals, vehicles, electric boxes, roads, light poles, etc., produce additional "bright areas"

in infrared images. This is especially true during the summer time. Also, the image intensities of the same object are not uniform and are adversely affected by dismount orientation, clothing and accessories. There is less image definition when the temperature of the background environment is similar that of the target. The intensity range of infrared images is generally more limited and consequently offer lesser quality data as compared to the visible range [16].

    2.3.3   Near and Short-wave Infrared.   Near infrared (NI) and short-wave infrared (SWIR) imagery present another option for dismount representation. While they do not offer the benefits of detecting thermal emissions, they have been proven useful in skin detection (Fig. 2.7) and face detection applications.

Figure 2.7: Original imagery from the 1080nm, 1580nm, and RGB cameras used for skin detection [16].

    2.3.4   Hyperspectral Imagery.   Hyperspectral images are typically used for geological surveys, because they offer richness of spectral data which provides several advantages over the other methods. Hyperspectral cameras take an image using several hundred wavelengths, ranging from visible though the near infrared, typically 400 - 2500nm with an approximated bandwidth of 10*nm* for each channel [34]. The light source curve (most of the time the Sun) and the absorption features of the atmosphere dominate the general shape of the spectrum from a hyperspectral system. The Sun's light peaks in

the green wavelengths and decreases towards longer and shorter wavelengths. The atmosphere absorbs light at wavelengths that correspond to the absorption characteristics of the constituent gases, such as nitrogen, oxygen, carbon dioxide, and water vapor. The peaks and valleys of a spectrum not due to the Sun or the atmosphere reveal information about the chemical composition of the spectrum being examined. Since every material has a unique spectrum, an analyst can look for diagnostic features from hyperspectral data [11]. This additional information allows analysts to examine characteristics and identify a possible nature of the imaged materials, as seen in Fig. 2.8. A standard hyper-spectral image can be thought of as a cube, where the X-Y plane is the two dimensional image, and the Z plane are the wavelengths divided in bandwidth sections.
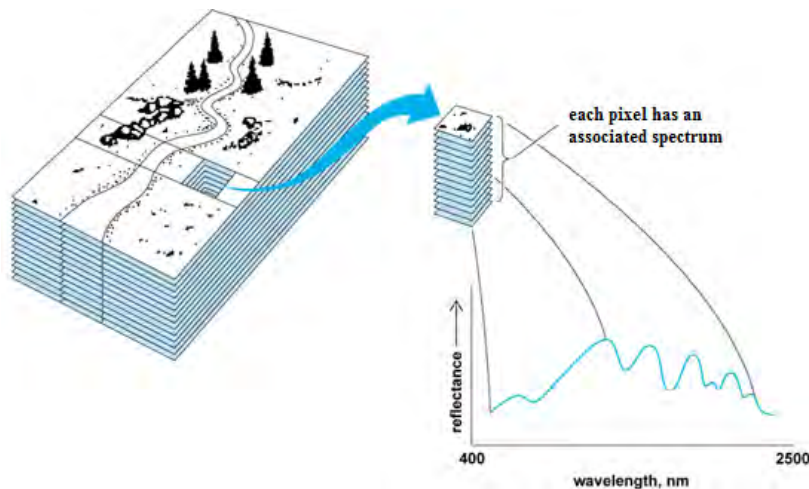
Figure 2.8: Representation of a hyper-spectral image. Each spatial element has a continuous spectrum that is used to analyze the material composition [11].

Hyperspectral imagery contains a lot of information about the material being imaged. Different materials respond differently at various wavelengths. Analyzing a single pixel throughout a hyper-spectral image provides important information regarding the material content in the image at that pixel. These signals can be used to discriminate between multiple classes of materials in images as demonstrated in [15] for clothing material, [12]

17

skin detection and for ground materials. One shortcoming of hyper-spectral sensing is that the spatial resolution is often worse than panchromatic sensors. This trade-off between spectral and spatial resolution arises in the sensor design as a result of the need to maintain imaging sensitivity at the finer spectral resolution of the hyper-spectral sensor [26].

2.4 Pixel Mixing

In order to create a robust dismount model that accurately represents common image acquisition, an understanding of "mixed" pixels is necessary. A mixed pixel is when one pixel contains several different features or classes as shown in 2.9. This leads to the spectral response at a pixel being a mixture of the underlying classes.
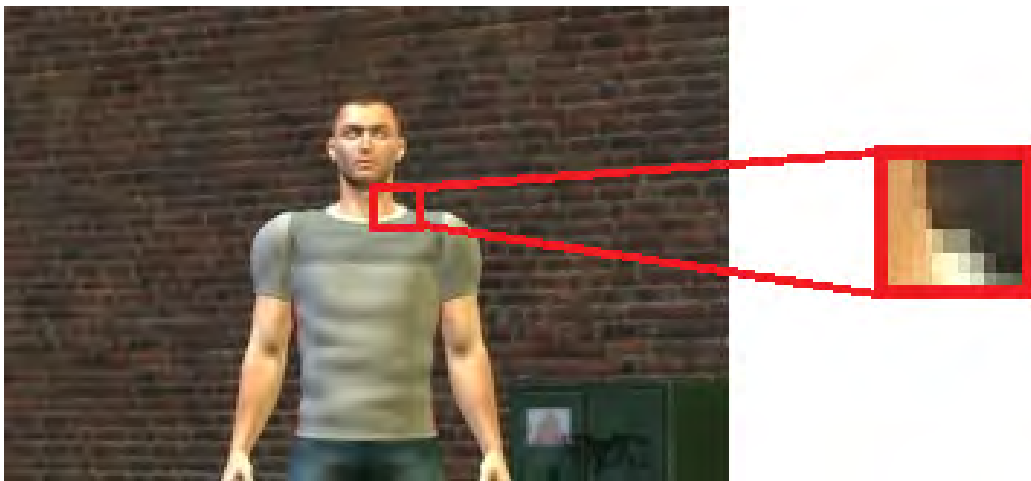
Figure 2.9: Mixed Pixels at class edge boundary between skin and brick background end-members (some shirt pixels are also mixed).

Most of the current studies in the area of remote sensing research have proposed several techniques for the un-mixing of pixels. There is not much information on the mixing of pixels. The purpose of this thesis is to generate a dismount model, therefore the use of techniques for un-mixing pixels are applied in order to mix pixels. There are two major approaches to mixed pixel classification: the linear and the non-linear approach.

2.4.1   Linear Mixture Model.   The simplest and most used approach is a linear mixture model (LMM) [5]. This approach models the linear combination of boundary members or end-members. The linear mixing model relies on two major assumptions,

1. The spectrum of a mixed pixel is a linear combination of the spectra of the constituent pure classes.

2. The spectral proportions of the pure classes reflect the area class proportions.

Linear Mixture Model (LMM) is defined as:

$$x_i = M f_i + e \tag{2.1}$$

where, M is an N x C matrix, its columns represent the spectra of the different end-members present in the image. $x_i = (x_1, x_2, ..., x_N)^T$ are the image values in the ith band, $f_i = [f_1, f_2, ..., f_C]^T$ is the proportion of each pixel within each class type C. N represents the number of features, C is the number of classes, and e is the error or bias.

LMM has two major constraints in regards to the proportion values f_i,

$$0 \leq f_i \leq 1 \text{ and}$$

$$f_1 + f_2 + ...f_N = 1$$

2.4.2   Non-Linear Methods.   The other pixel mixing approach is the non-linear model. This approach utilizes several statistical techniques for pixel mixing, i.e. Nearest-Neighbor, Bayes and Kernel methods [23].

2.5   Summary

This chapter outlines several dismount representation approaches and their application towards dismount identification and characterization. The chapter also describes various alternatives of imagery data which allows researchers to accomplish

dismount representation and characterization. Finally, the LMM algorithm for mixing pixels is discussed. The details and the methods implemented for a computer aided multi-data dismount model are presented and described in Chapter III.

3   Methodology

The methodology for the conception of a computer aided multi-data dismount model is discussed in this chapter. The dismount model description is explained in detail. Future developers and users will be able to modify and expand this structured design. The chapter also discusses the methods, processes and algorithms used to design a modeled scene. The first topic is the architecture and top level design. The top level design allows understanding on how the dismount model was developed and the various modules of the model are individually described. These modules include,Pixel Map, Background Model (Nature, Man Made Elements), Dismount Model (Face, Feet, Torso, Hand, Legs, Neck and Arms), Signature Attachment (at each element in the pixel matrix), End Member Detector and Pixel Mixing (LMM).

3.1   Top Level Design

Figure 3.1 shows the procedures for the development of a modeled scene. The first step is to create the pixel map. The pixel map is used to describe each pixel according to its location in a modeled scene, as explained in Section 3.2. Once the pixel map is completed, each pixel, or group of pixels of a class (i.e. shirt, hair, etc.) is assigned a signature. The type of multi-data signature to be attached to the pixel map depends on the end user modeling needs and the modeled imager capability. These multi-data signatures can be RGB, multi-spectral, hyper-spectral, imager specific or any other required bandwidth.

After the signatures are applied to the map in its entirety, pixel mixing by way of linear mixing process is accomplished. Pixel mixing creates a representative model of current imagine technologies. To implement pixel mixing the boundaries of each modeled element needs to be identified. For this purpose, end-member finder (edge detector)
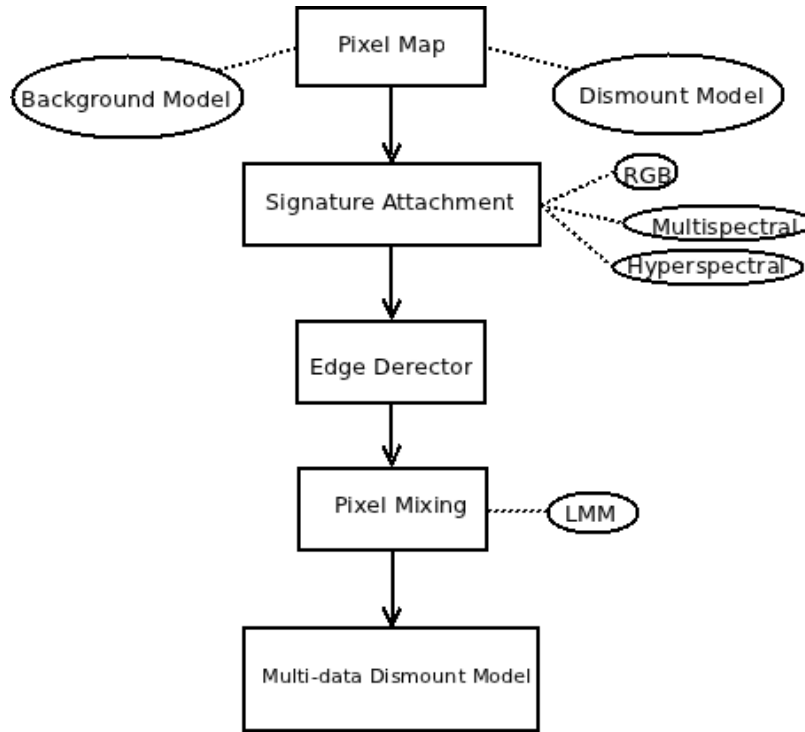
Figure 3.1: Multi-data fusion dismount model elements.

algorithm is employed. After signatures are attached and end-member pixel elements are mixed, the multi-data dismount model is complete.

3.2   Pixel Mapping

In order to develop a modeled scene the creation of a pixel map is necessary. The pixel map consist of an m x n matrix. Therefore, if the user needs an image that is 800 by 600 pixels, the dimensions of the pixel matrix can be adjusted to render that image ($m = 800$ and $n = 600$). The x axis corresponds to the horizontal dimension and the y axis corresponds to the vertical dimension as shown in Fig. 3.2.

This pixel mapping matrix allows for the representation of several distinctive classes in the image. The value of each element in the matrix represents a class (i.e., brick, grass, skin, shirt, etc.) in the scene. For example, in Fig. 3.2 a basic pixel map is shown. For this example, the matrix is a 25 x 25 element matrix with several classes represented.

Figure 3.2: Pixel Map of a 25 by 25 image. Each entry in the matrix represent a class in the scene. For example, the pixel in location (1, 1) represents background (coded as 0) and pixel in location (12, 6) represents skin (coded as 1) as seen in Table 3.2.

For each pixel map (matrix), a *legend*, which describes each mapped class, must be included. Table 3.2 shows the legend for the pixel map that belongs to the pixel map in Fig. 3.2. The legend describes the class of each pixel in the scene and identifies which signature is being modeled in the pixel map. For example, the pixel in location (1, 1) coded as 0 represents a background class and pixel in location (12, 6) represents a skin class pixel, coded as 1. Based on this legend and the pixel map, signatures can be attached as desired by the user.

3.2.1   Pixel Map Development.   There are several alternatives for the development of a pixel map,

- Manual Model Development (MMD)

- Modifying an Existing Model (MEM)

23

Table 3.1: Pixel Map legend codes for Fig. 3.2.

Elements	Maps to:
0	Background
1	Skin (Face/Head)
2	Skin (Neck)
3	Clothing (Torso)
4	Skin (Arms)
5	Clothing (Lower Torso)
6	Clothing (Legs)
7	Skin (Hands)

- Algorithmic Model Generation (AMG)

Manual Model Development (MMD) refers to the creation of a two-dimensional (2D) matrix (i.e. m x n), where each entry represents a pixel in the image according to its location (x, y) in the pixel matrix. MMD can be created using several computer programs that allow manipulation of 2D matrices, like Microsoft Excel or Libre Office.

The second alternative is to modify an already created model (MEM). The model can be modified for several reasons. One is to incorporate new variations or details, and second, to add new desired elements (i.e. additional dismounts, cars, trees, etc.). This is possible by changing the pixel map. For example, if a change to the pixel map in Fig. 3.2 is needed, it can be easily achieved by changing elements of the matrix with a different number according to the legend (Table 3.2) or by adding extra elements to the pixel map and to the legend.

The third option is algorithmic modeling or matrix manipulation (AGM). Algorithmic Modeling refers to the creation of a pixel map by the use of algorithms. Predefined modeled structures can be easily modified, adjusted and created with algorithms and

clustering schemes. There exist several programs (i.e. MATLAB, Java, Phyton) that allow clustering identification, matrix management, manipulation and programming.

3.3   Model Overview

The development of the model consist of several stages. The first stage, is the "basic" stage. The most basic scene, for the purpose of this thesis, must include the dismount and background models. Later, on further stages, more elements and details like for example: extra dismounts, face details, cars, buildings, trees could be added to the scene to represent a different situation as desired by the user. Another alternative to further enhance the model is to move the angle of view in the scene (sidewise view, top view, back view), to create shadowing effects or to completely remove the dismount(s) to model an aerial to ground photograph or a geological survey.

3.3.1   Dismount Module.   A morphological model using body outline and body composition by parts is implemented in order to create the dismount model. The dismount elements to be modeled consist of the following: head or face, neck, torso, hands, arms, legs and feet.

The combination of all these create a complete dismount. By modeling each dismount part separately, we can accelerate the assignment of a specific signature to a dismount section. During the second stage, details and variations can be incorporated to each section separately. This enhances the creation, modification and reuse of models. For example, if the user desires the hands to be of a specific skin color or size, the requested color signature could be assigned to the entire hands section instead of going pixel by pixel. Once a dismount is completed it could be used in different scenes with minimum changes.

3.3.2   Background Module.   Every modeled scene needs a background. For the basic stage, the background model is a plain black background (Fig. 3.3). Note that this

25

"basic" background can later be changed with any wanted signature. The signature could be of: RGB, multispectral or hyperspectral nature as needed by the user (Fig. 3.1). Modifying elements in the background section will make possible the simulation of different environments and background objects. Alterations to the background are done by changing the pixel map and adding the respective signatures to be attached to the model.

3.4 Signature Attachment

Once the pixel mapping is complete, signatures can be attached according to the pixel map's legend. The pixel map legend allows the creation of a rendered scene from a repository of signatures, which can be assigned to each element of the pixel map.
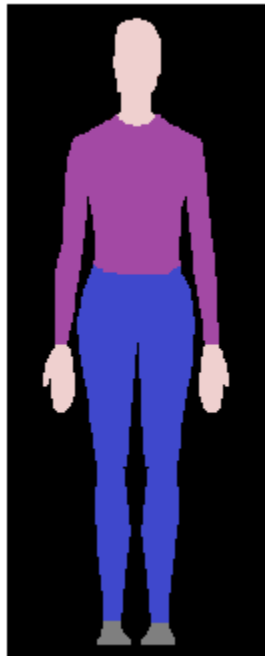
Figure 3.3: Basic scene with RGB signature attached.

For example, in Fig. 3.3 the following RGB colors are assigned to the pixel map:

1. [63 72 204] a variation of blue to the legs to represent jeans,

2. [255 218 230] to represent skin in head and hands,

3. [163 73 164] to represent a purple shirt,

4. [127 127 127] for gray shoes,

5. [0 0 0] for the black background.

If the user needs a different signature, (i.e., a hyperspectral signature), it is attached using the same scheme. The only difference is that a hyperspectral signature has more elements per pixel location instead of three as does the RGB vector [red, blue, green] (Fig. 3.4).
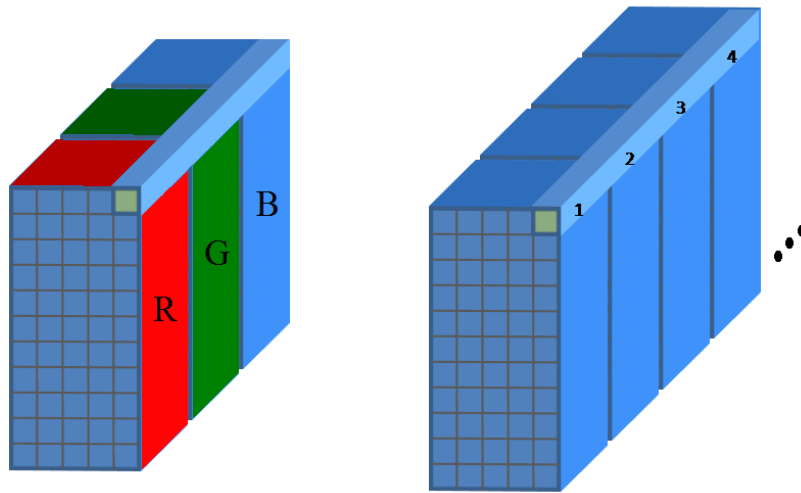
Figure 3.4: Pixel map showing RGB signature (left) vs hyper-spectral signature (right). The hyper-spectral signature have more elements than a RGB which has only three.

For the purposes of this thesis, the signatures will be gathered with an spectroradiometer (ASD) [21] and from several hyperspectral images acquired with a hyperspectral camera (HST) [35]. Signatures can also be acquired using previously created models or from a signature repository. This depends on the requirements for the

model (i.e., if the model is of hyperspectral nature then the signatures needs to be hyperspectral). Environmental effects also need to be considered for the selection of the appropriate repository of signatures. Discussions of the different considerations when selecting a hyperspectral signature are mentioned in Section 4.3.

3.4.1 Signatures from Spectroradiometer. The spectroradiometer used for the acquisition of hyper-spectral signatures is a FieldSpec 3 Portable Spectroradiometer from ASD Inc. [21]. The spectroradiometer consists of a hand-held contact probe connected to a spectrometer with a fiber optic cable (Fig. 3.5). The contact probe contains its own illumination source (artificial) which covers the Visual (VIS), Near Infrared (NIR) and Short-Wave Infrared (SWIR). The system is calibrated by placing the contact probe, with its illumination source, against a calibrated reflectance panel with a known reflectance. Once the system is calibrated, the contact probe is placed against materials such as dismount's skin and clothing. Reflectance for the different wavelengths in the VIS, NIR, SWIR, can be then collected.

For this thesis, signatures were obtained from the same individual by getting measurements from the dismount's skin, sweatshirt, jeans, shirt, hair and the background objects as identified in Section 4.1. Figure 4.2 shows the location points where the signatures were taken using the spectroradiometer.

Per the data sheet of the ASD FieldSpec 3, the spectroradiometer offers a spectral range from 350 nm to 2500 nm with a spectral resolution of 3nm at 700nm and 10nm at 1400/2100nm. The amount of electromagnetic energy received by the spectrometer at a specific wavelength can then be associated with the reflectance of a material at that wavelength. Figure 3.6 show the various reflectance signatures acquired with the spectroradiometer and used for the Multi-data dismount model, shown in Fig. 4.10.

28

Figure 3.5: ASD FieldSpec 3 Spectroradiometer used to acquire reflectance signatures to populate the dismount model [21].

3.4.1.1   ASD Spectroradiometer Data Processing.   The data acquired from the ASD spectroradiometer has to be post-processed in order to match the data acquired with the HST hyperspectral camera. This is due to the fact that the resolution capabilities and the wavelengths ranges covered by the camera does not match those acquired when using the spectroradiometer, as mentioned in Section 3.4.2 and Section 3.4.1 respectively.

The process of modifying the spectrometer data is accomplished by data averaging to match sampling interval and resolution of the HST. By effectuating this process over all the acquired spectroradiometer signatures, the data formatting is accomplished. Now the signatures from both sources (spectrometer and hyperspectral camera) can be compared.

This process allows the evaluation of the feasibility of accurately modeling a scene using hyperspectral data acquired by the ASD to resemble those signatures gathered with a hyperspectral camera of a real scene. This discussion is documented in Section 4.3. The resulting signatures after the ASD spectroradiometer data adjustment is completed and the data acquired with the HST hyperspectral camera is shown in Fig. 4.5 trough 4.9.
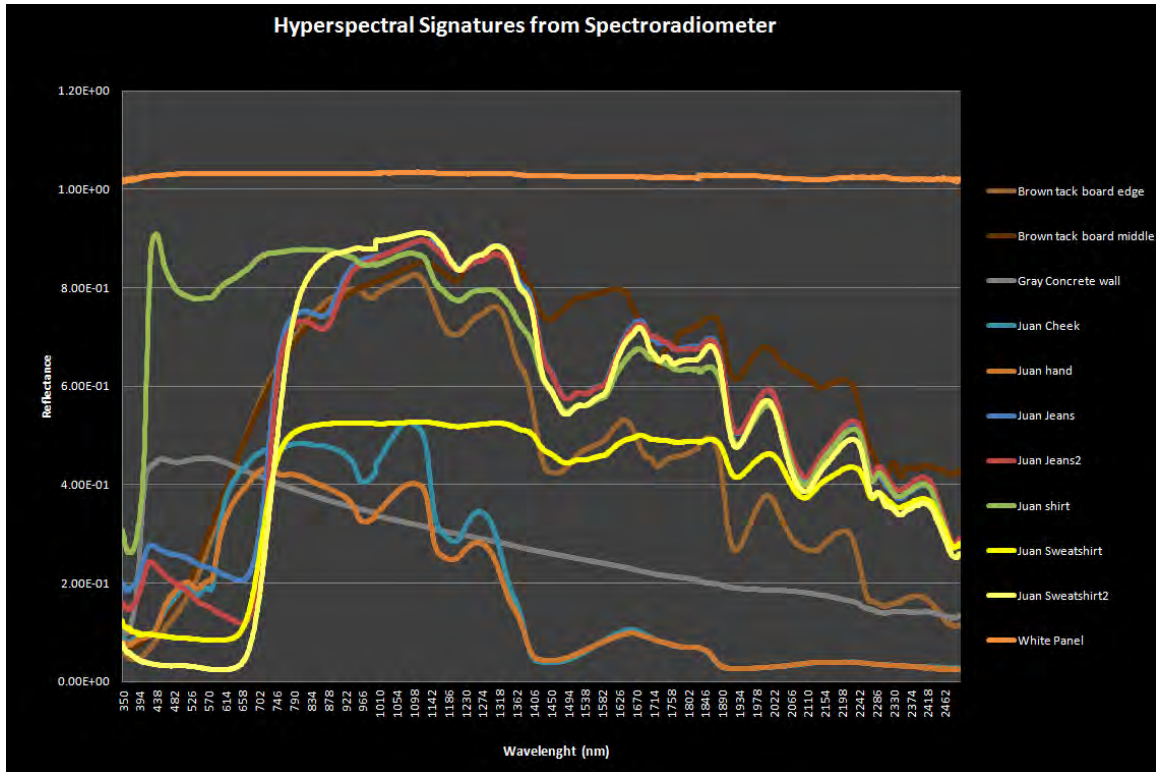
Figure 3.6: Dismount's Hyperspectral Signatures from ASD FieldSpec 3 Spectroradiometer. These reflectance signatures are used to populate the dismount model.

3.4.2 Signatures from Hyperspectral Camera. The hyperspectral image is generated by HyperSpecTIR (HST) hyperspectral camera. After capturing the image, the data is processed according to the post-processing specifications of the device. Signature collection location points are identified in Fig. 4.2 (similar location for all collection sources).

The HyperSpecTIR camera HST shown in Fig. 3.7, is comprised of a pair of bore sighted grating spectrometers each operating in a portion of the electro-optic (EO) spectrum between 450 nm and 2450 nm. The visible and near-infrared (VNIR) spectrometer assembly operates over the range of 450 nm to 900 nm. The short wave infrared (SWIR) spectrometer assembly operates over the range of 900 nm to 2450 nm. These two spectrometers are oriented such that they view the scene through a series of

optical quality mirrors. The instantaneous field-of-view (IFOV) of the instrument is a line image of 1 mR by 256 mR oriented along the along-track axis.
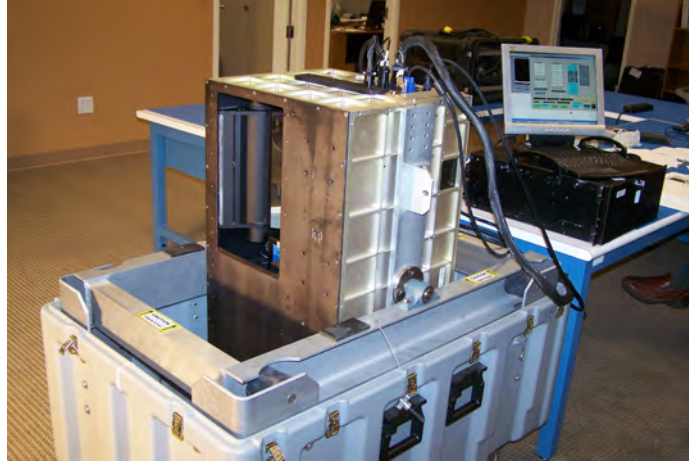
Figure 3.7: HyperSpecTIR hyperspectral camera [35].

Each collection is 256 pixels in the y-direction (along track) by a variable number of pixels in the x-direction (cross-track), dependent on desired resolution (1m res. = 150 pixels/ 3m res. = 550 pixels). Each data cube produced by the system covers the wavelengths between 450 - 2450 nm, with about 248 selectable bands; 240 of which are data imagery bands and 8 of which are allocated to GPS footer data which is later used in post-processing and data verification. This GPS data is disregarded in the image analysis for this thesis. Of these 240 data imagery bands, several are redundant as a result of the spectral overlap between the two spectrometers and are removed during the post-processing [35].

   3.4.2.1   HST Data Processing.   After the raw data is collected, further data processing is required. The post-processing programs included in the HST system take care of this step [35]. When the processing is completed, data cubes are created and hyperspectral signatures (in radiance units) are obtained from the scene.

In order to translate the HST hyperspectral data radiance to reflectance values for model population and multi-data signature comparison purposes additional post-processing is required. The data output from the HST hyperspectral imager is in radiance, which is the total electromagnetic energy reflected from the target which includes environmental effects (atmospherical, green house, etc.) and is dependent on the intensity of the illumination source. Empirical line correction (ELC), is used to find the corresponding reflectance for each pixel in the image and is calculated based on the white and gray calibration panels (identified in fig. 3.8).

Figure 3.8: White and Gray reflector panels used for reflectance calculations (red squares).

To calculate the empirical line correction the following inputs are required:

- location of the reference panels (Fig. 3.8),

- the hyperspectral signatures of the panels from the HST hyperspectral image (Fig. 3.9) and,

- the hyperspectral signature specifications from the manufacturer for both calibration boards (Fig. 3.10).

Once they are obtained, the determination of the reflectance signatures from the HST radiance data can be found for each pixel.
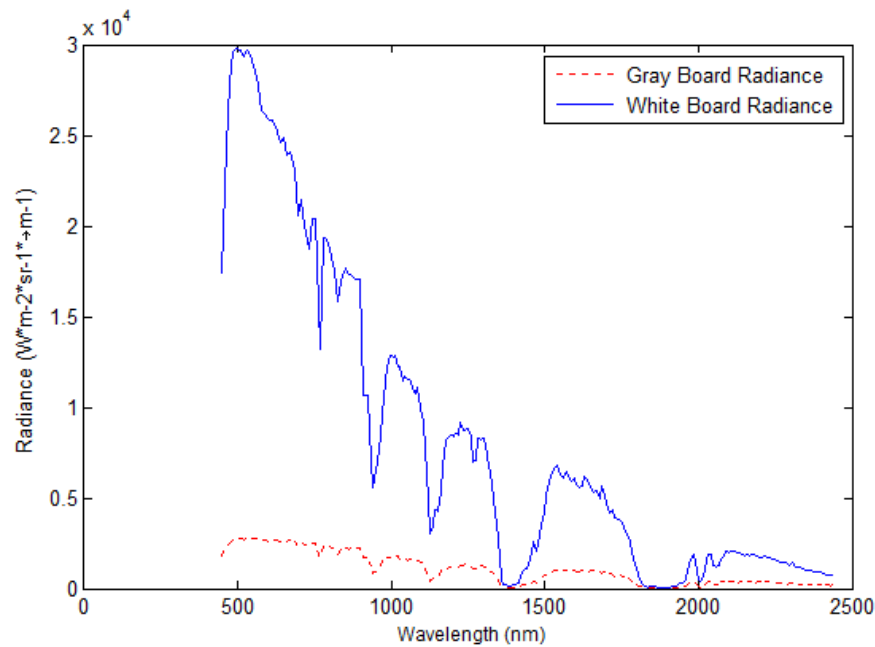
Figure 3.9: White (blue line) and gray (red line) boards radiance from the HST hyperspectral camera before ELC processing.

The corrected signatures of the white and gray boards are shown in Fig. 3.11. It can be noticed that these match those given by the manufacturer (Fig. 3.10). The hyperspectral image in its entirety can be processed using the developed ELC. Now reflectance comparison between the Multi-data signatures can take place. In summary, the use of Empirical Line Correction and the reference true reflectance measurements (manufacturer) from the white and gray boards (Fig. 3.10), are necessary to determine the corrected reflectance measurements. Hence, for further enhancements to the thesis it is necessary that the two reference reflectance boards are included in the pictures.
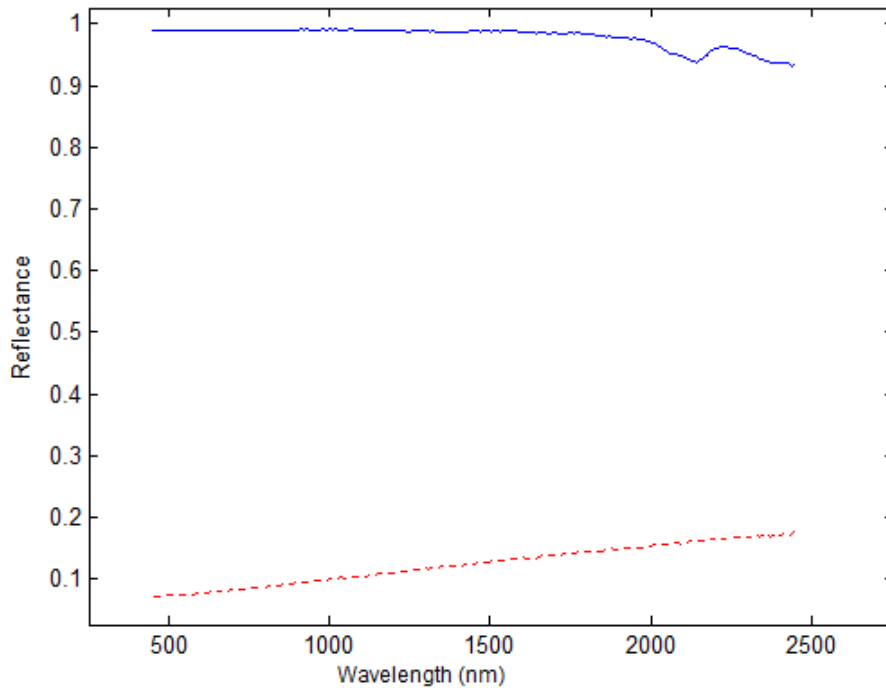
Figure 3.10: Reference reflectance specification from the manufacturer. These signatures represent the true wavelengths responses. The blue line corresponds to the white panel reflectance and the gray panel is represented the red line.

3.5 End-Member Pixel Mixing

In order to conservatively represent current hyperspectral image acquisition capabilities, end-member pixel mixing is incorporated in the model. This is accomplished by the use of linear mixture model (LMM). One of the effects of LMM is that it introduces variation and certain level of ambiguity to the multi-data model. This ambiguity will later make its effect in material classification. To mix the end-members the edges of the dismount and background elements need to be identified. Section 3.5.1 provides a brief description of the end member finding method used in this thesis. Once the edges are located, LMM (Section 2.4.1) is applied to all of the end-members elements at those locations making an element pixel mixing based on user defined class proportions.
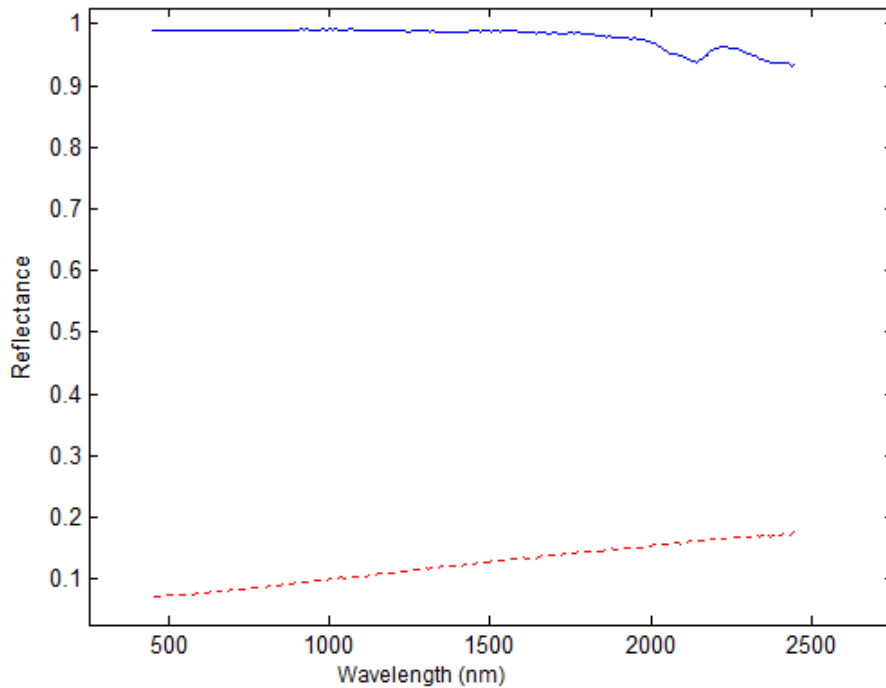
Figure 3.11: The resulting hyperspectral reflectance measurements after the image is processed using ELC for the white panel (blue line) and gray (red line) panel.

3.5.1 Edge Detector Module. There are several ways to find an edge in an image. This section provides a brief insight and description of the edge detection approach used in this thesis. The problem of edge detection is of great importance in image analysis. As mentioned in Section 2.1.1.2, edges characterize a dismount outline and are therefore useful for segmentation and identification of dismounts in a scene.

An edge in an image is a jump in intensity [13]. The cross section of an edge has the shape of a ramp. An ideal edge is a discontinuity (i.e. a ramp with an infinite slope). Many researchers [27, 40] have used an error function or smoothed step as the simplest form of an ideal step edge model for modeling the effects of blur and shading in practical application.

The localization of edges is used to identify end-members of an element in the model. For example, in Fig. 3.2, it is desired to mix the pixels that are at the boundary (end-members) of the dismount's head (coded as 1) and the background (coded as 0) to recreate a mixed pixel between those materials and mimic current imagery technology. The edge detector algorithm (Fig. 3.12) is able to identify this end-members and then apply LMM (Section 3.5) to the model. An example of the procedure is described below,

```
function End Member Mixing Algorithm (Pixel Matrix, Hyperspectral
                 Signatures, LMM Percentages)
   returns: (Pixel Mixed Multi-data Model)
   inputs: Pixel Matrix, (m x n) multi-data model matrix
           Hyperspectral Signatures, classes signatures to be mixed
           LMM percentages, mixing amount per class (user defined)
   for 1:Size(Pixel Matrix)
       Identify end-class-members pixels
       Determine end-members classes (2 or more) in all directions
           (up, down, left, right).
       Mix end-members classes using LMM (Section 2.1)
           with user defined percentages.
   end for
```

Figure 3.12: Edge Detector Algorithm with LMM implementation.

Once the signatures are attached and end-member pixels are mixed the dismount model is complete. If additional details, dismounts or background elements need to be added, the process needs to go back to the pixel map modification stage. The pixel map will have to be adjusted to reflect new changes, signatures are added and reattached, and pixels are mixed. This will incorporate any new changes to the model if needed.

3.6 Summary

This chapter described the various components and algorithms for the creation of the Multi-data dismount model. In the next chapter specific details of the implemented model, the specifics about the hyperspectral signatures applied and algorithmic parameters are

provided. A basic comparison of the hyperspectral signature reflectance measurements (ASD and HST) for model population is conducted and documented. Also, the results obtained and dismount models are presented.

4 Experimental Results and Analysis

This chapter documents the dismount and scene modeling process, obtained results and their analysis. The developed multi-data dismount model is presented side-by-side with the hyperspectral images signatures for comparison. As part of the analysis, a straight forward comparison, in reflectance terms, between modeled data and hyperspectral imagery is also conducted. At the same time, the chapter describes the processes for attachment of hyperspectral signatures from two different sources; the first being hyperspectral signatures captured with HST camera, and the second, signatures acquired with a Spectroradiometer (ASD).

The chapter begins by discussing the acquisition and nature of the hyperspectral signatures used in this thesis. Then it justifies the use of certain algorithms and describes specifics about the pixel map development process, signature attachment and the created multi-data model. The last section of this chapter presents an analysis of the results to include an hyperspectral dismount model comparison between: 1) model populated with signatures acquired with the spectrometer [21], 2) and an image acquired with the hyperspectral camera [35]. Also, throughout this chapter; advantages, disadvantages and possible uses for the computer aided multi-data dismount model are documented.

4.1 Data and Signature Acquisition

In order to achieve the research goals discussed earlier, several hyperspectral data collections were necessary. This hyperspectral data came from several dismount images taken with two hyperspectral cameras the HyperSpecTIR hyperspectral [35] and PHIRST Light II cameras [17]. For the case of the HST hyperspectral images, they were acquired in a sunny day with an environment temperature of about 38 degrees Fahrenheit and natural lighting (Sun), shown in Fig. 4.1. The PHIRST Light II collection took place in an indoor setting (artificial lighting) with a temperature of about 70 degrees Fahrenheit.

Reflectance measurements used to populate the dismount model were acquired with the Analytical Spectral Devices (ASD) FieldSpec 3 Spectroradiometer [21].

Figure 4.1: Image captured with HST hyperspectral camera, taken in the open (Sun), semi-urban environment in a sunny day.

To populate the dismount models, signature acquisition points are identified from each source (spectrometer and hyperspectral cameras). Figure 4.2 shows these points.

Figure 4.2: Location of signature acquisition points (yellow squares) for the two signature acquisition methods (spectroradiometer and hyperspectral camera).

The hyperspectral signatures varies depending on reflectance characteristics, nature of the material and source of illumination. There is a need that all of the points have similar reference location and units of measurement for multi-data comparison. The signature elements for the population of the dismount model are the following,

- background 1 (cork board)

- background 2 (white calibration board)

- dismount's hair

- dismount's sweatshirt

- dismount's pants

- dismount's shirt

- dismount's skin (face/cheek)

The fact that the location of the signature points are similar (same element), awards the ability to compare multi-data models with similar locations from the various sources (Section 4.3). As well as to compare the representation ability of a "natural" scene versus the modeled scene (Section 4.3.1).

4.2   Results and Model Development

The developed model for representation of the dismount and background in a scene, imitates the image taken with the hyperspectral camera. The main reason behind this scheme is to be able to conduct a basic study of the ability of a computer aided multi-data model to represent a dismount's morphological form as well as ability to represent a "natural/real" situation or scene acquired with a hyperspectral camera (Section 4.3.1).

The model's *pixel map* is developed from the images seen in Fig. 4.1 for HST and Fig. 4.2 for PHIRST Light II cameras. This is accomplished using an algorithmic

modeling generation (AMG) as explained in Section 3.2. Clustering and grouping the various elements (Section 4.1) using morphological body outline and body composition by parts, give us a basic template for the pixel map. The pixel map or scene matrix that resulted from this approach is shown in Fig. 4.3 for the HST model and Fig. 4.4 for the PHIRST Light II model.
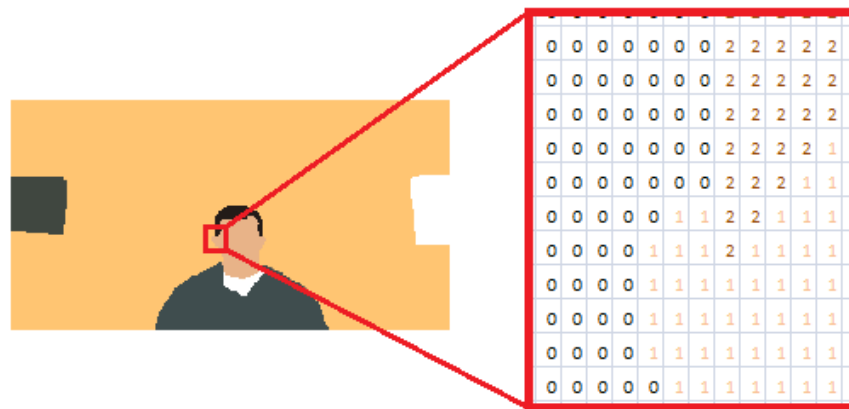
Figure 4.3: Pixel map to mimic image taken with HST hyperspectral camera. The pixel map is the result of clustering the scene image following AMG and morphological body outline and body composition by parts.

After the scene matrix is completed values are assigned to the pixel map and the *pixel map's legend* is created (i.e. Section 3.2). For example, all of the skin sections were grouped as a skin and given a value of *1* in the pixel map. The pixel maps legend for both models is shown in Table 4.1.

The next step according to the system architecture (Fig. 3.1) is the incorporation of signatures. For this thesis the signature repository consist of hyperspectral signatures acquired from the ASD Spectroradiometer (Section 3.4.1.1).

Figure 4.4: Pixel map to mimic image taken with PHIRST Light II camera. The pixel map is the result of clustering the scene image following AMG and morphological body outline and body composition by parts.

Table 4.1: Pixel Map legend codes for Fig. 4.3 and Fig. 4.4.

Elements	Maps to:
0	Background
1	Skin
2	Hair
3	Shirt
4	Sweatshirt

4.2.1 Hyperspectral Model. The hyperspectral signatures acquired with the ASD Spectroradiometer can now be processed and attached to the pixel map according to the pixel map's legend. Figures 4.5 trough 4.9 shows the resulting model from the attachment of the spectrometer signatures to the scene model (Fig. 4.3). The figures include the signature plots from the HST hyperspectral camera (left) and the Spectroradiometer

reflectance signatures attached to each element in the model (right) with their respective location.

Figure 4.5: Cork board model, populated using spectrometer data in the right (after wavelength matching, Section 3.4.1.1) vs. hyperspectral imagery in the left (after HST data processing, Section 3.4.2.1) and their respective attached reflectance signatures.

4.2.2   Signature Attachment using Imagery Data.   A second alternative for the database used to populate the computer aided multi-data model, is to use signatures acquired from a imager. Signatures can be acquired from an image by selecting a specific section or location where the desired element is located and populating the model.

One of the disadvantages of hyperspectral sensors is the need to incorporate *atmospheric correction algorithms* [11]. Atmospheric effects need to be taken into consideration when signatures are attached to the model using signature directly captured form imagery data. The nature of the hyperspectral signatures will affect the results of the model. The use of this type of signatures present a concern, where environmental

43

Figure 4.6: Cheek (skin) model, populated using spectrometer data in the right (after wavelength matching, Section 3.4.1.1) vs. hyperspectral imagery in the left (after HST data processing, Section 3.4.2.1) and their respective attached reflectance signatures.
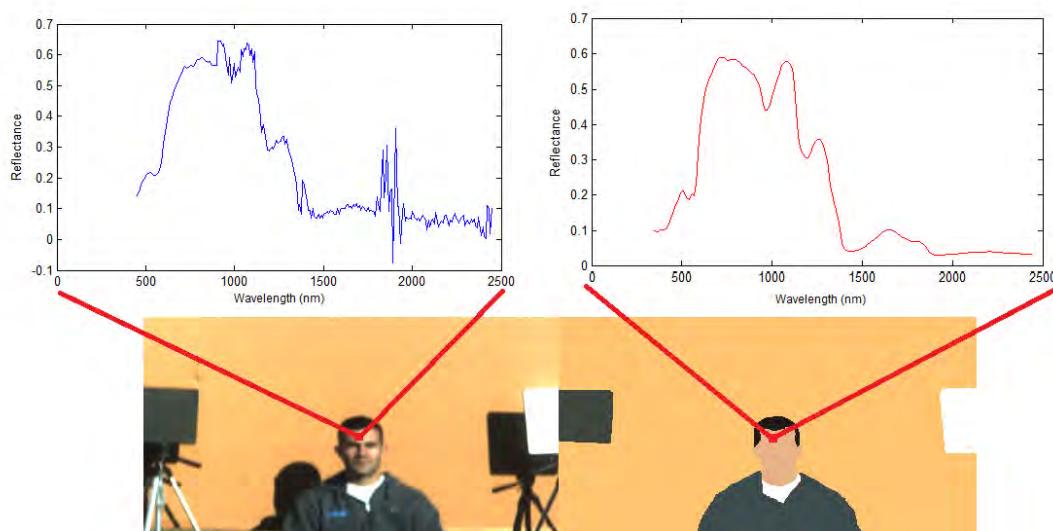
Figure 4.7: Forehead (skin) model, populated using spectrometer data in the right (after wavelength matching, Section 3.4.1.1) vs. hyperspectral imagery in the left (after HST data processing, Section 3.4.2.1) and their respective attached reflectance signatures.
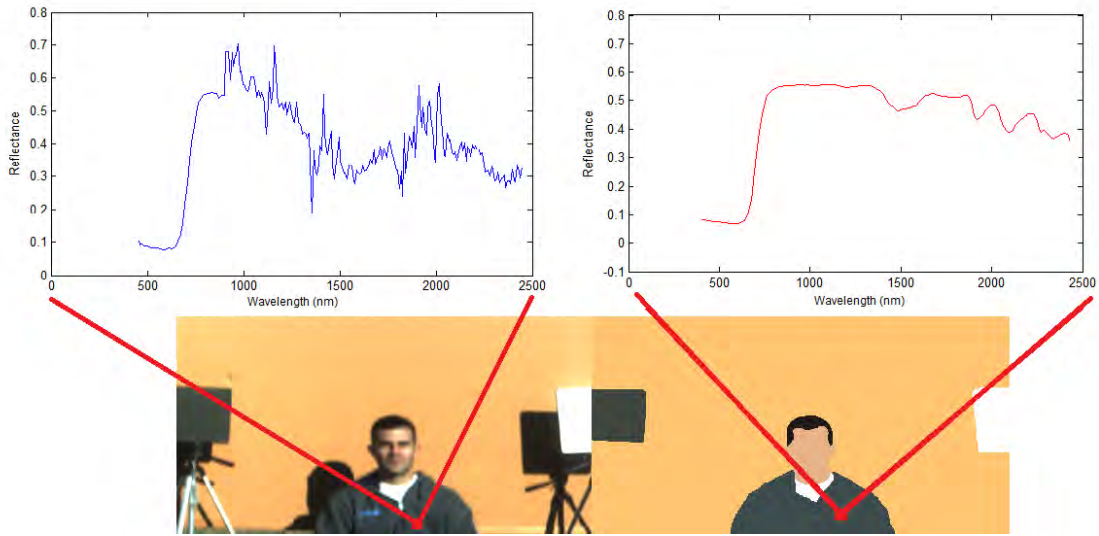
Figure 4.8: Sweatshirt model, populated using spectrometer data in the right (after wavelength matching, Section 3.4.1.1) vs. hyperspectral imagery in the left (after HST data processing, Section 3.4.2.1) and their respective attached reflectance signatures.
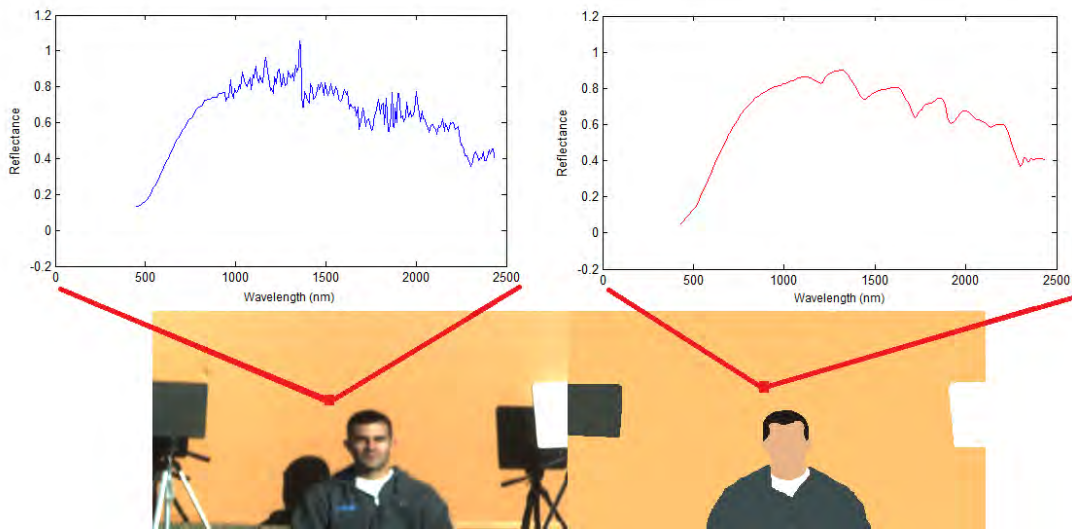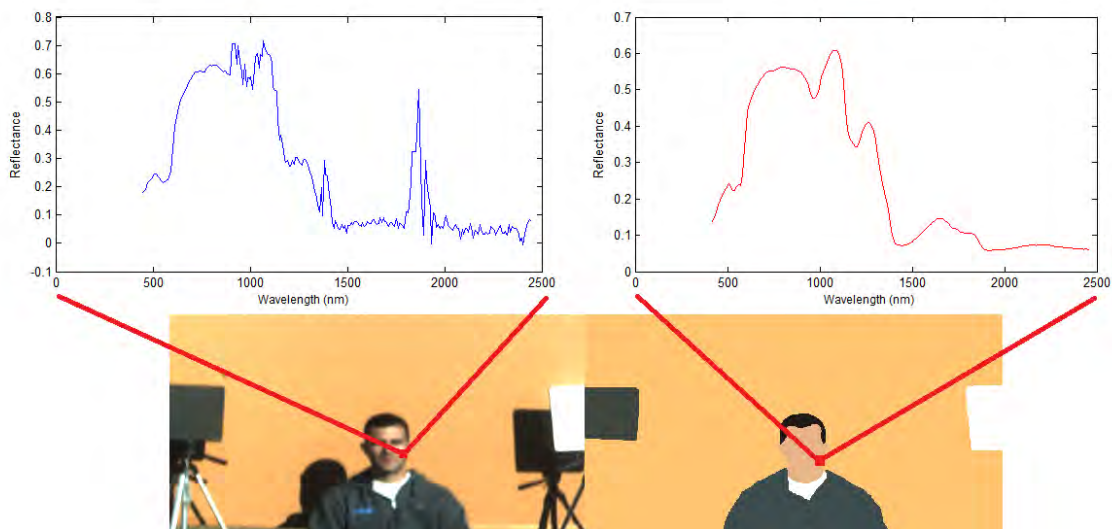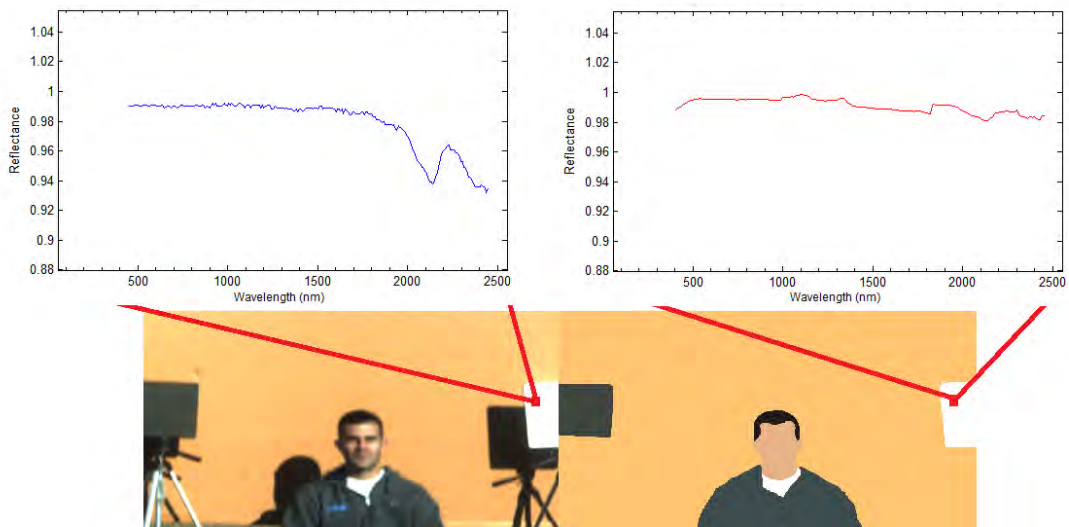

Figure 4.9: White board model, populated using spectrometer data in the right (after wavelength matching, Section 3.4.1.1) vs. hyperspectral imagery in the left (after HST data processing, Section 3.4.2.1) and their respective attached reflectance signatures.

45

phenomena (i.e. atmospheric effects, temperature, humidity and others) are existent during the image collection event. These effects are certainly embedded in the hyperspectral signature and must be taken into consideration if environmental effects play a role for employment and use of the created model. A better option will be to model the environmental effects into the acquired data from the Spectroradiometer and then populate the model.

4.3   Analysis

This section studies the ability of a computer aided multi-data model to recreate a scene where a dismount is present. It accomplishes this by comparing the created hyperspectral dismount model data versus data taken from a hyperspectral camera image. The evaluation and comparison of the difference in reflectance between the two approaches is, as well, documented in this section.

This comparison takes place in order to verify the feasibility of the model to resemble images taken with a hyperspectral camera. Additional analysis is necessary to conclude with exactitude the nature of the different effects that affect the direct resemblance of the model and hyperspectral HST camera data, and the accountability of the same. Even though, a hint of these possible difference effects is given during the analysis for future consideration.

At the same time, supplementary measurements like: spatial resolution, atmospheric effects, illumination, shadowing, are examined for the model's signatures, as well as for the image acquired using the hyperspectral camera. Finally, throughout this section some of the advantages and disadvantages of having a computer aided multi-data model versus a hyperspectral imaging system are mentioned.

4.3.1   Resemblance of Model vs. Hyperspectral Image.   For the purpose of this thesis the created model mimics the image taken with the hyperspectral camera. The

objective of this approach is to demonstrate the ability of the model to represent a hyperspectral image utilizing a pixel map. Figures 4.10 and 4.11 shows two hyperspectral images taken with a hyperspectral cameras HST (RGB) and PHIRST Light II Camera and their respective modeled scenes (RGB) side by side.
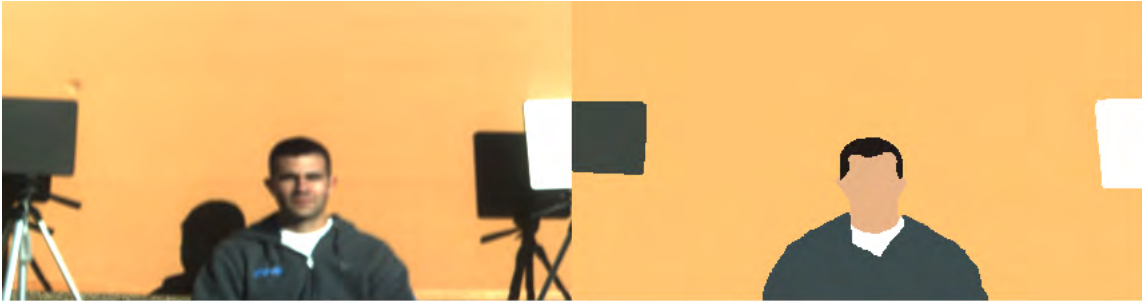
Figure 4.10: Model emulating hyper-spectral image taken with HST Camera [35].

Figure 4.11: Model emulating hyper-spectral image take from PHIRST Light II Camera (BAE Systems) [17].

It is observable that both models as well as the modeled scenes (Fig. 4.10 and Fig. 4.11 respectively), have similar dismount outline and contain the same background

elements. The signatures attached to the model were of RGB nature and was done to demonstrate the ability of variation of such, as seen in Fig. 4.11 right side.

When the models are reviewed against the hyperspectral images, it is also observable that details are lost in Figs. 4.10 right side. These *loss of details* may be of importance for the purposes of dismount identification. For this occasion, the modeled scene will have to be enhanced to comply with the requirements. It is also noticeable that the "real" image from the hyperspectral camera HST (Fig. 4.10 left) is *out of focus*, which also may present a concern for dismount identification purposes. An alternative solution to these intricacies is to use regular (RGB) cameras for the objective of dismount identification and similar applications. For the study of dismount characterization and dismount detection, the dismount model is of great advantage when compared to hyperspectral camera. The computer aided multi-data model allows rapid modification of scenes, change of signatures, enhancement, dismissal or modification of environmental effects, replication of images, model reuse and many others.

Another observable difference is that in the modeled scene there are *no shadows* present. At the present time, this capability was not implemented in the dismount model, but shadows can be simulated and incorporated on the model in the next developmental spiral. Other noticeable differentiation is that *illumination changes* are not captured by the model. The changes in illumination could be modeled by adjusting the amplitude of the attached signature where the illumination is different (i.e. specularity). Again these changes to the model can be added in the next evolution of the model.

Every illumination source has its own characteristic signature. The *nature of the illumination source* or source characterization signatures, can be modeled and implemented in the model to obtain radiance signatures. This could be done after the signature acquisition (reflectance) from ASD is obtained. The reflectance signatures could be adjusted to represent different illumination sources as needed by the user. All of these

enhancements can be implemented in the near future if required by the user and applications.

4.3.2   Signal Comparison Image vs. Modeled Scene.   The model selected to conduct the signature analysis is that from the HST hyperspectral camera as seen in Fig. 4.10. In order to have a basic comparison of the model, a straight forward hyperspectral signatures similarity breakdown between model data and HST (imager) data was executed. This comparison is conducted by selecting the modeled elements signatures and imaged signatures from the hyperspectral imager. Both signatures are compared in reflectance terms excluding water absorption bands (shadowed in light blue) for difference percentage calculations. This percentage of difference reflects a measurement of dissimilitude between each other. Not to be exchanged with signal error.

For this comparison analysis, both signals are plotted and displayed conjunctly in the same graph. The model's signature is collected from the ASD spectroradiometer (red dashed line) and the imager signature is taken with the HST hyperspectral imager (blue line). The respective signal post-processing adjustments for both ASD and HST are carried out according to Sections 3.4.1.1 and 3.4.2.1 respectively. Difference measurement are calculated at each wavelength band and averaged over the entire wavelength range (400 nm to 2500 nm) to obtain the percentage of difference for each modeled element (i.e. sweatshirt, skin, etc.). For this calculations environmental effects (atmospherical, green house, water and CO_2 absorption) around 1400 nm and 1900 nm wavelength bands were dismissed for observations and conclusion purposes.

As observed in Fig. 4.12, the difference between the collected hyperspectral signature from HST (blue line) and the modeled hyperspectral signature signal (red dashed line) for the *white board* is minimum. The calculated difference between the signals is 1.25%. The most noticeable difference between the two signatures take place

49
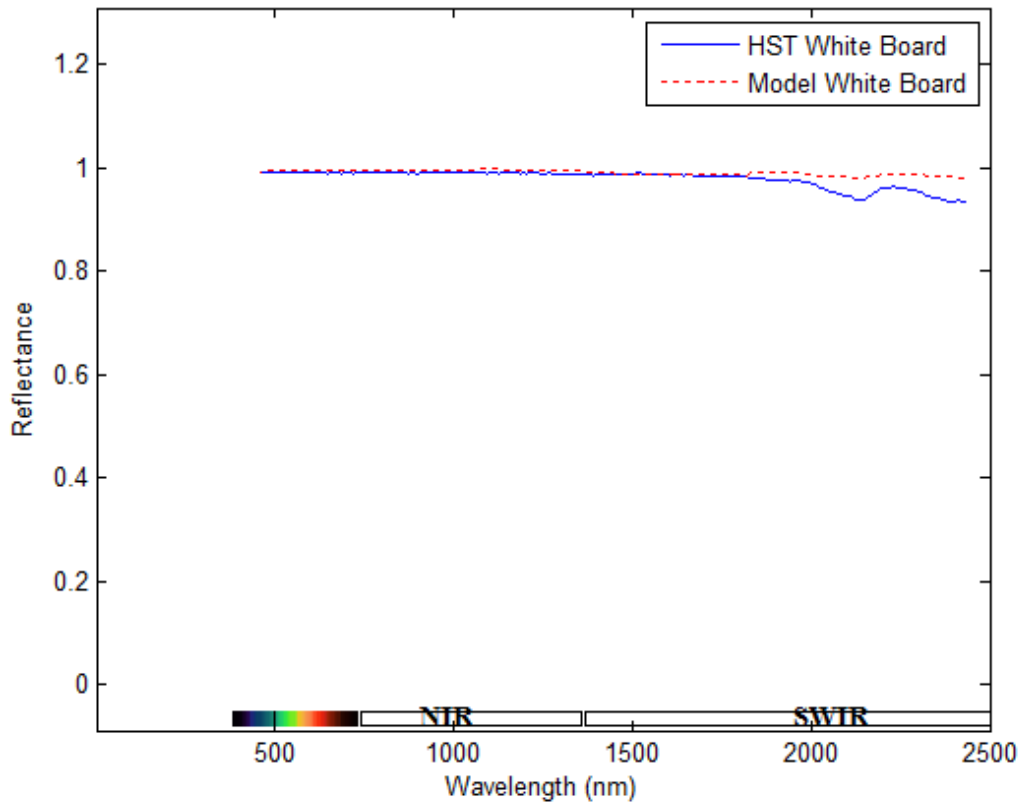
Figure 4.12: Modeled signature (red dashed line) and actual imager output (blue line) for the *white board*, with water absorption frequencies shadowed in light blue.

after the 2100 nm wavelength band. This could be attributed to internal parameters in the machines or environmental effects.

For the case of the *cork board* signatures, the calculated difference for the selected pixels (Fig. 4.13) is 2.4%. It can be noticed that the HST data (blue line) has more variation and is noisier than the model's signature for this background element. This could be attributed to atmospheric effects as well as imager effects. The resemblance of the two signals is evident and they have the same shape.

For the *white shirt* area, the signals are similar and follow the same outline. The calculated difference percentage is 11.4%. This apparently higher percentage could be an
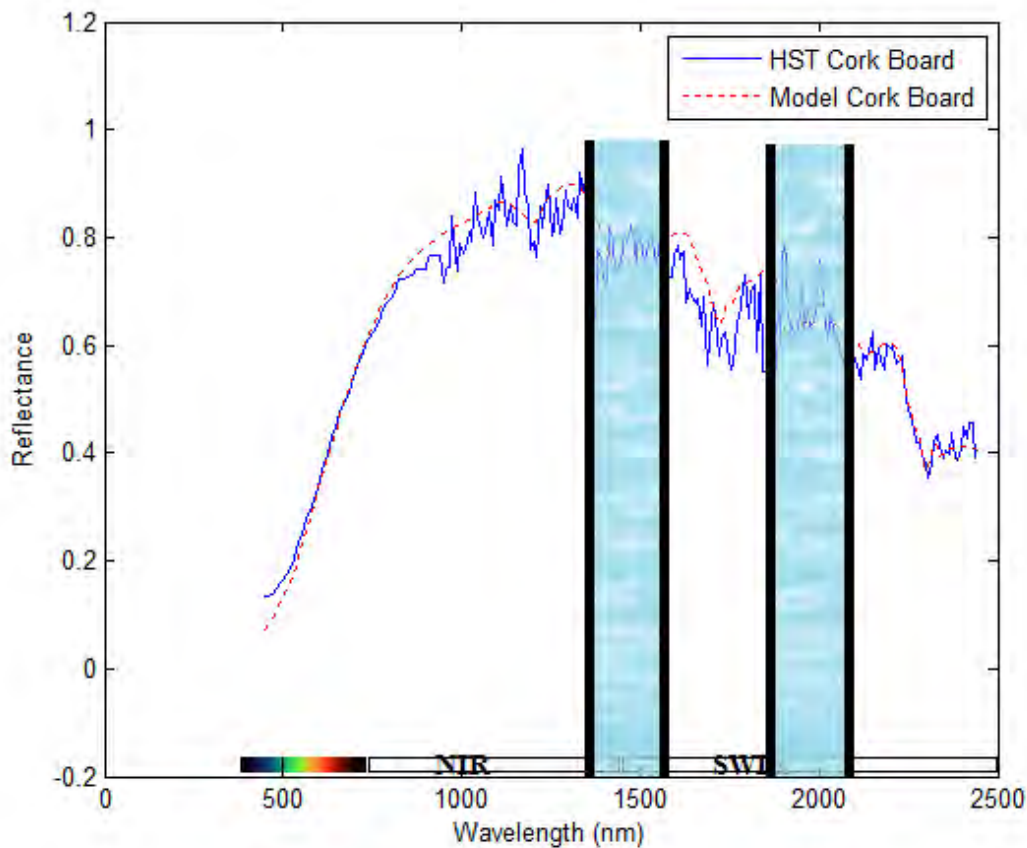
Figure 4.13: Model's hyperspectral signature (red dashed line) and actual imager output (blue line) for the *cork board*, with water absorption frequencies shadowed in light blue.

effect that the measurement taken with the Spectroradiometer was acquired with the shirt on the dismount body and skin/heat properties may have influenced the final result. Additional research may infer the specifics about this effect.

There is a difference of 7.67% between the Model and the HST signatures for the *sweatshirt* pixels. The majority of this difference takes place after 900 nm wavelength. Some of the causes for this might be because environmental temperature at the time of the capture was colder (38 degrees) than that of the ASD (70 degrees) or it could also be imager specific effects.

Figure 4.14: Model's hyperspectral signature (red dashed line) and collected hyperspectral signature (blue line) for the *shirt*, with water absorption frequencies shadowed in light blue.

The signature of the model for the *cheek* area is 3.32% different than that of the collected image. Although, both follow similar signal outline. It is noticeable that the blue signal (HST) changes drastically after 900nm, which can be referred to as a *imager effects*. This imager effects are noticed in all the signals taken with the HST hyperspectral imager. This might be caused because the HST hyperspectral imager possess two spectrometers (Section 3.4.2.1). At 900 nm the imager moves to the second spectrometer and the gain or amplitudes might be different between the two. The signature up to this point of 900 nm is smooth (minimum environmental effects) and closely resemble that of the model. After this point it becomes noisier, but still follows the general form of that of the model.

Figure 4.15: Model's hyperspectral signature (red dashed line) and collected hyperspectral signature (blue line) for the *Sweatshirt*, with water absorption frequencies shadowed in light blue.

In the case of the *forehead area*, which has similar shape of that of the cheek area (skin), both signatures (HST and model) resemblance each other and follow the same signature shape. The difference between them is about 2.54%. Again, the imager effects are also noticed around 900 nm of wavelength. The HST signature becomes unstable after this measurement, but it still follows the general characteristics of the model and viceversa. This instability or noise may be attributed to atmospheric effects, imager focus and the previously mentioned imager effects.

4.3.3   Signal Comparison Mixed Pixels in the Image vs. LMM Pixel Mixing Modeled Scene.   After finding edge element members, *pixel mixing* is possible. Linear Mixture Model was the approach used for pixel mixing in this thesis (Section 2.4.1). In regards to signature comparison (mixed pixels model vs. mixed pixels collected), edge
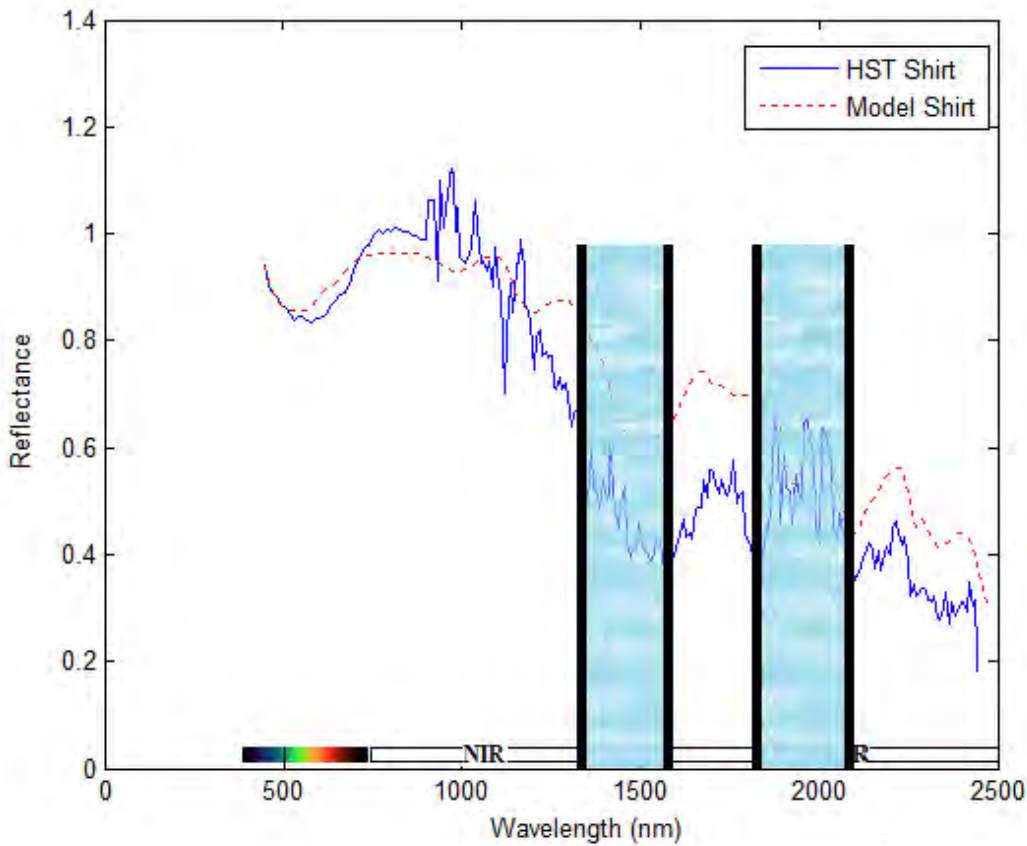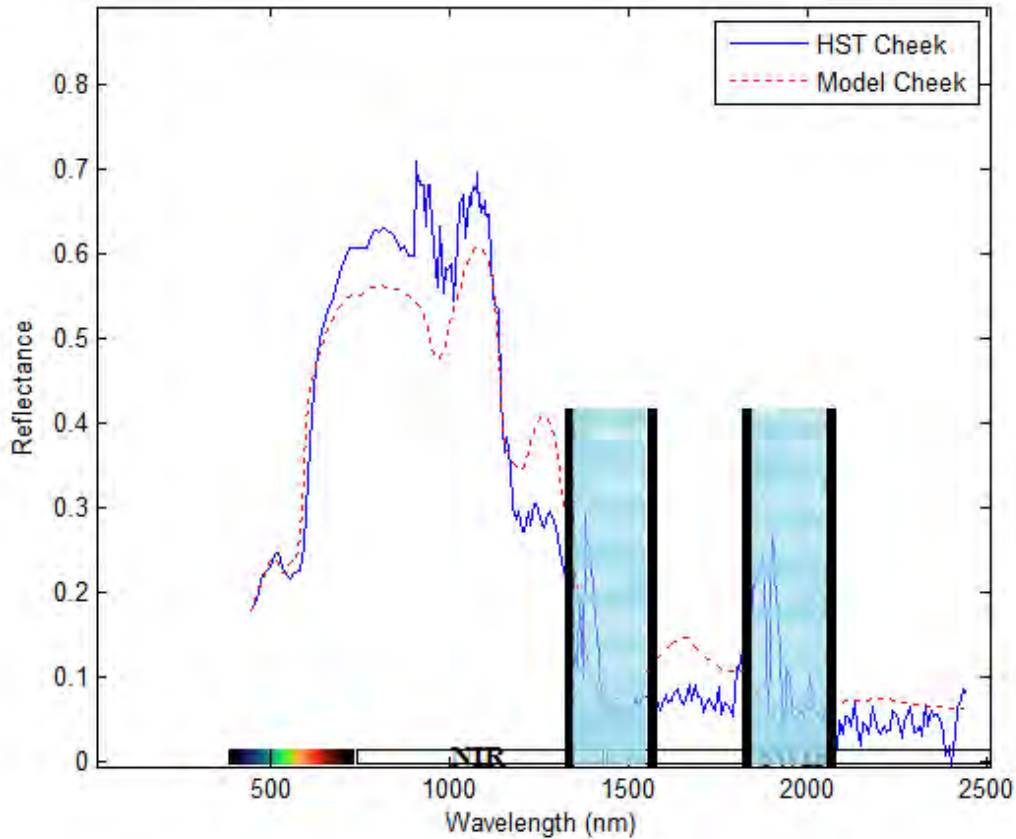
Figure 4.16: Model's hyperspectral signature (red dashed line) and collected hyperspectral signature (blue line) for the *Cheek (skin)*, with water absorption frequencies shadowed in light blue.

member pixels or mixed pixels in the hyperspectral image (from the HST) where visually identified and used to verify the calculated pixel mixing performance. For example, in Fig. 4.18 a mixed pixel in the original hyperspectral image (HST) is identified at the skin and cork board boundary region. This pixel contains skin and cork board at sub-pixel levels.

After computing the LMM using 50/50 between cork board and skin respectively, the resulting signature is shown in Fig. 4.19 (red dashed line). Considering that the selected "mixed" pixel from the HST (blue line) is taken from a visual inspection of the figure it is
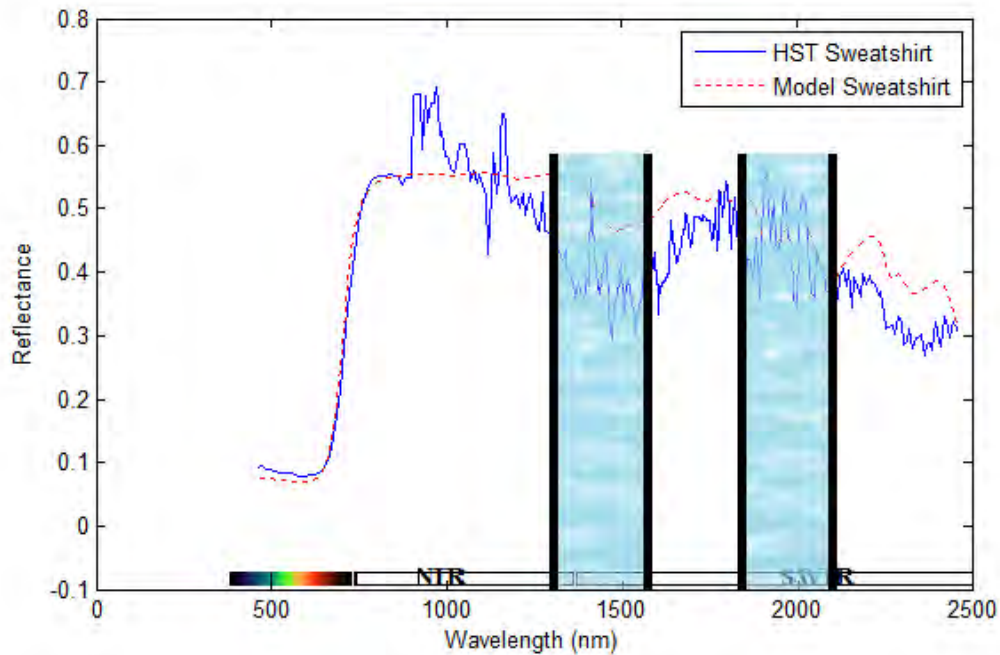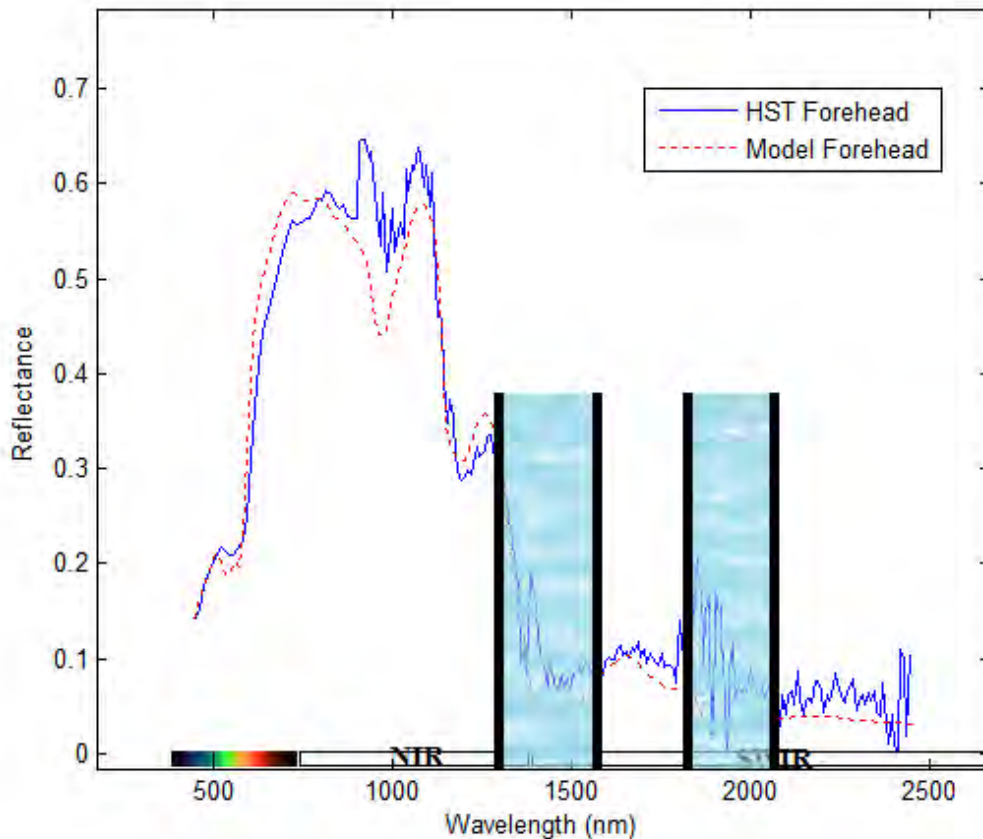
Figure 4.17: Model's hyperspectral signature (red dashed line) and collected hyperspectral signature (blue line) for the *Forehead (skin)*, with water absorption frequencies shadowed in light blue.

observable that both follow the same outline. The calculated difference for this case is 8.35% after elimination of absorption bands (marked in blue).

In the case of a mix between sweatshirt signature and cork signatures, results are shown in Fig. 4.20. Again, imager effects and environmental effects are present (HST). However, both signals, with a LMM mix of 50% sweatshirt and 50% cork signature modeled mix and HST (mixed pixel), follow the apparent same shape. The calculated difference between the two signals (model vs imager) is of 3.82%.
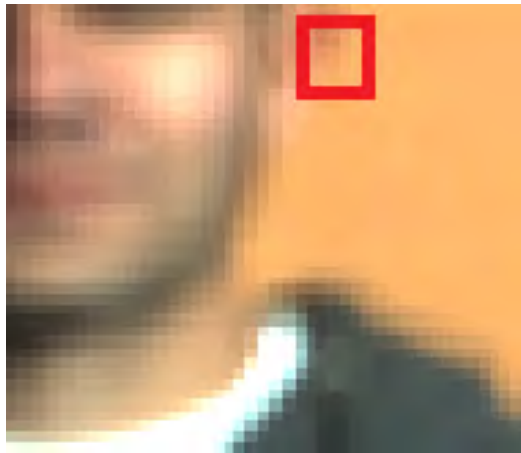
Figure 4.18: Mixed Pixels between Skin and Cork Board (inside red square).
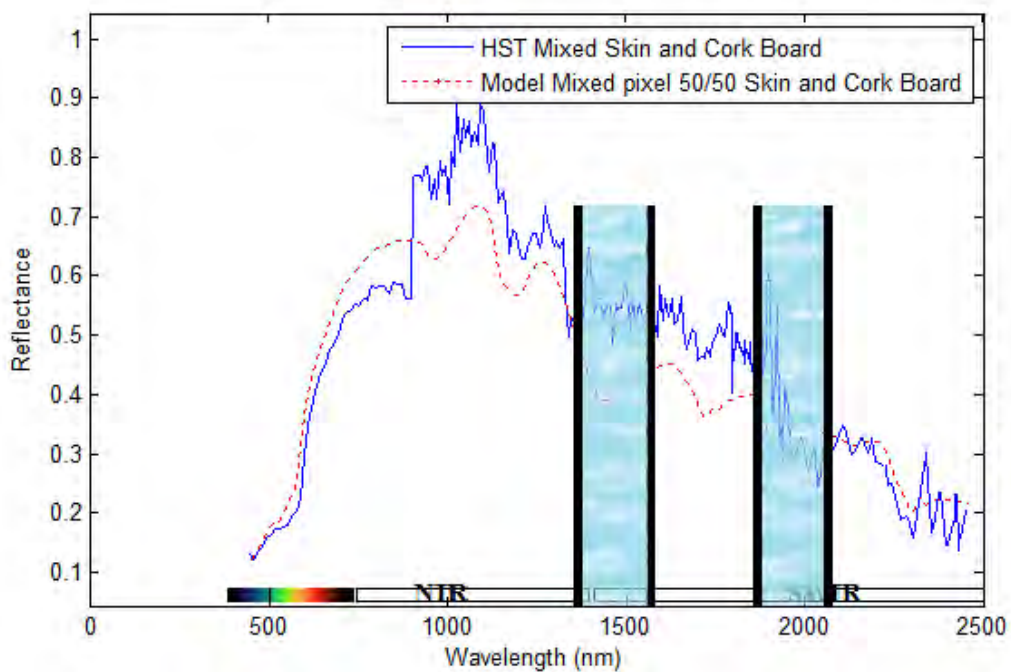
Figure 4.19: Model's hyperspectral signature after LMM pixel mixing of 50% skin and 50% cork board signature (red dashed line) vs. collected hyperspectral signature imager output for a *mixed pixel skin and cork board region* (blue line), with absorption frequencies shadowed in light blue.
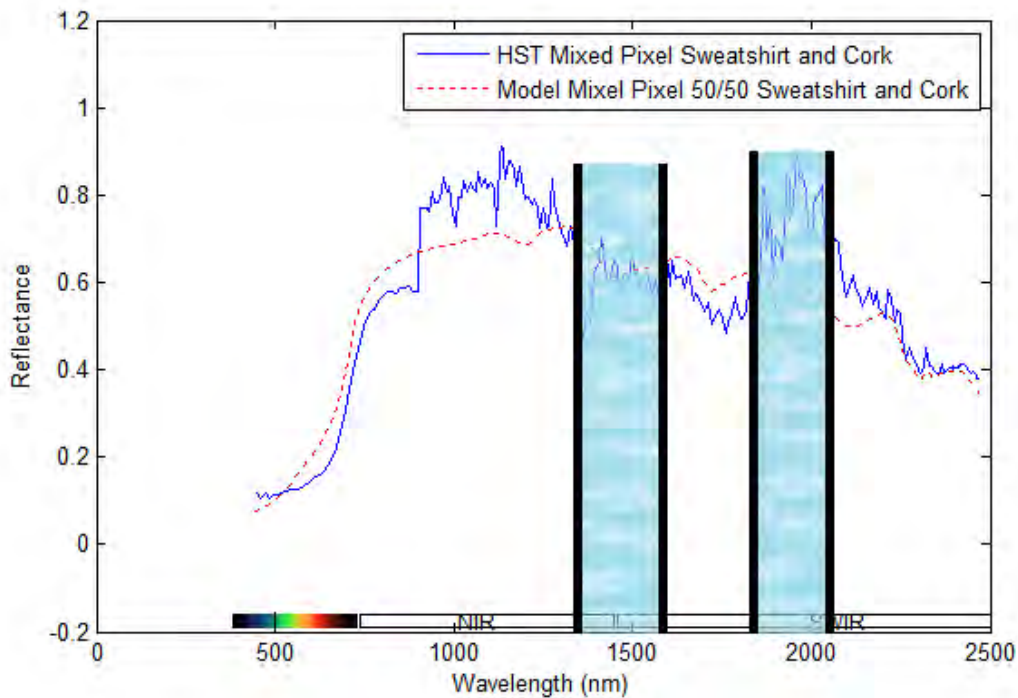
Figure 4.20: Model's hyperspectral signature after LMM pixel mixing of 50% sweatshirt and 50% cork board signature (red dashed line) vs. collected hyperspectral signature imager output for a *mixed pixel sweatshirt and cork board region* (blue line), with absorption frequencies shadowed in light blue.

Figure 4.21 shows the results of a 50% white board reflectance signature and 50% cork board reflectance signature mix (red dashed line) and the signature of a mixed pixel collected with the HST hyperspectral imager. The difference between the signatures is 8.60%. Environmental and imager specific effects may have caused this difference between the two signals.

Finally, a pixel where various elements (skin, white shirt, sweatshirt and corkboard) are present is identified in the HST figure and modeled by using a LMM pixel mix with 25% skin, 25% white shirt, 25% sweatshirt and 25% corkboard. The obtained results are displayed in Fig. 4.22. It is observable that both signatures are similar and the calculated dissimilitude is 4.9%.
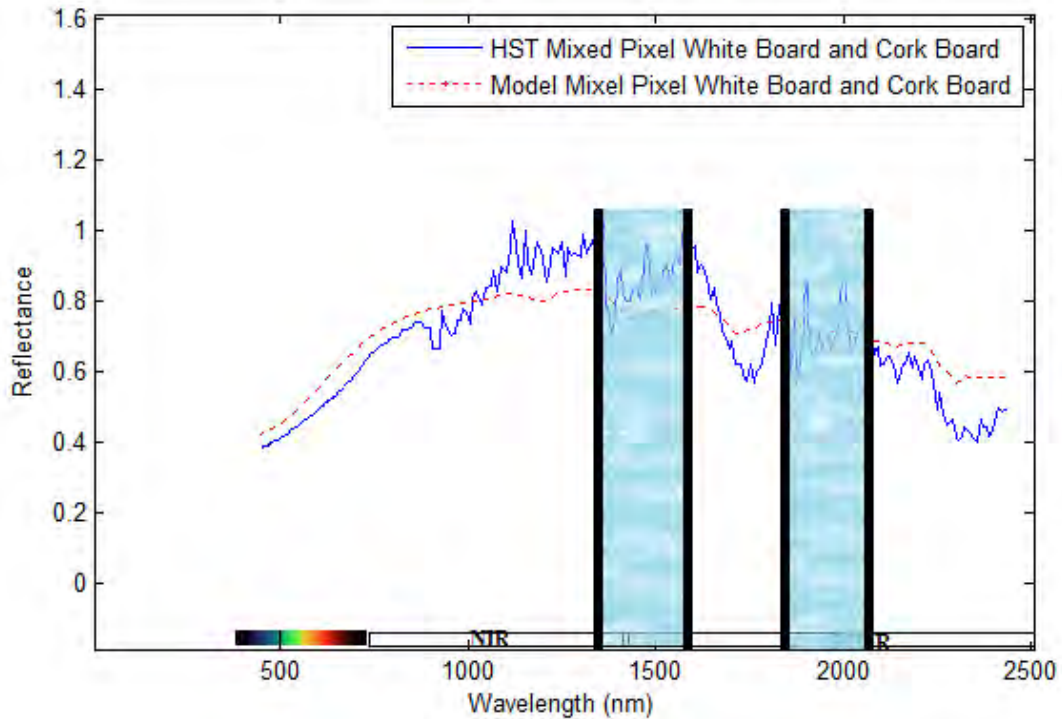
Figure 4.21: Model's hyperspectral signature after LMM pixel mixing of 50% white board and 50% cork board signature (red dashed line) vs. collected hyperspectral signature imager output for a *mixed pixel white board and cork board region* (blue line), with absorption frequencies shadowed in light blue.

After the comparison of difference between the modeled and collected signals, it is demonstrated that LMM is a substantiable approach towards pixel mixing. Environmental effects, as well as the imager specific effects will need to be modeled and studied in order to capture them in the dismount model if complete resemblance is necessary.

Other elements to be taken into consideration for the case of a multi-data dismount modeling in a scene, is the *spatial resolution*. Spatial resolution does not make a considerable effect on the illustration of the image. The main reason for this, is because the images were taken in a close proximity to the dismount. In the case there is a aerial
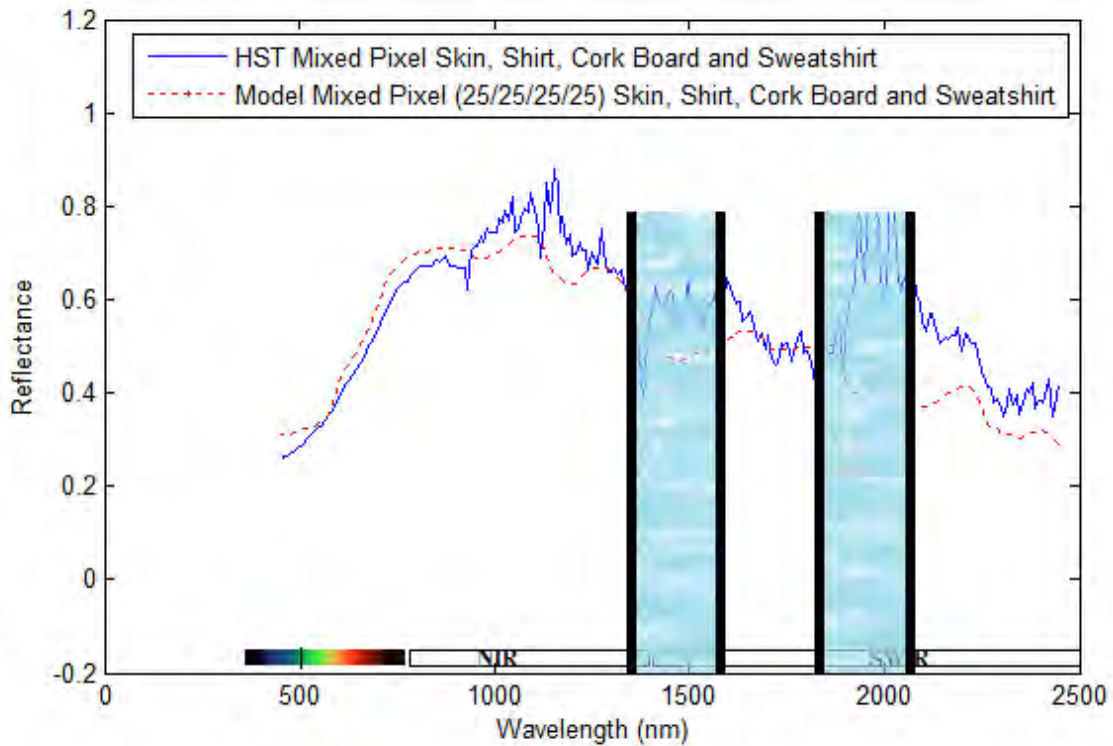
Figure 4.22: Model's hyperspectral signature after LMM pixel mixing of 25% skin, 25% white shirt, 25% sweatshirt and 25% corkboard signatures (red dashed line) vs. collected hyperspectral signature imager output for a *mixed pixel skin, white shirt, sweatshirt and corkboard* (blue line), with absorption frequencies shadowed in light blue.

collection or a collection where the resolution parameters of the systems are compromised, then the spatial resolution as well as the pixel mixing effects will be evident in the model.

One important observation from this signature comparison study is that hyperspectral imaging systems contain both quantitative and qualitative information, not only from the imaging elements (dismount, background, etc.), but *system dependent characteristics* (i.e. processing, data manipulation schemes). The wide range of possible hyperspectral imaging products prevent using a single or multiple metric(s) to characterize system performance in a general manner. The difference between the systems is the approach

taken here. Thus, the developed multi-data model suffers from hyperspectral imaging system inherited effects, we called imager effects.

5   Conclusion and Future Work

This chapter begins with a discussion of the research goals and the achievements accomplished by the development of a multi-data dismount model. Then a brief summary of results and analysis is presented. The final section covers the potential for future work to improve the developed computer aided multi-data dismount modeling scheme.

5.1   Summary of Methods and Conclusion

The purpose of this thesis was to create and demonstrate the feasibility of a systematic method to construct a computer aided multi-data fused dismount model for the demanding studies of dismount detection, characterization and identification. The developed system is built on a systematic architecture. This architecture allows the ability to represent a scene where a dismount is (or is not) present in a background. The model is capable of being adjusted to represent any scene required by the researcher. The dismount, sections of the dismount, as well as the background, can be modeled and amended to match the necessities of the researcher.

The main focus of the system is particularly in hyperspectral signatures to the dismount model. Hyperspectral imaging systems are being applied to a number of areas, including environmental studies and especially for defense purposes. Hyperspectral signatures uniquely capture spatial and spectral information, which allows the researcher to use these characteristics to detect and characterize dismounts.

The created dismount model is capable of reaching multi-data modeling advantages without the need of acquiring expensive imagery equipment and dedicated software. Therefore, with the described computer aided multi-data dismount model the researcher will be able to attach signatures to any desired modeled scene. These signatures represent current imagery equipment by the employment of LMM pixel mixing and by the further addition of atmospheric modeling and imager noise specific characteristics. Even though,

61

the last two have not been implemented in the current development, the model is able to resemble a hyperspectral image with minimal difference between the two (about 5%), as demonstrated in Section 4.3. All of the information required is contained within the dismount model, or can be furtherer incorporated in the multi-data model if necessary (i.e. signature with atmospheric, illumination, imager noise effects).

It is clearly demonstrated that the developed multi-data dismount model is capable of representing any desirable scene situation by the creation and employment of the pixel map, multi-data signature attachment and pixel mixing. Furthermore, the model allows the user to easily modify the posture, shape, location, size, position, multi-data signatures, as well as the modification of the background elements and characteristics in the scene. Multi-data signatures (i.e. hyperspectral, multispectral, RGB) are attached to the pixel map, and edge members pixels are located and mixed to generate the final modeled scene. By the employment of LMM and pixel mixing, the model is able to mimic current imaging technologies with a proven resemblance between hyperspectral signatures, mixed signatures and its imaged counterparts.

After hyperspectral signature analysis and model data versus imager data comparison, it is found that signatures acquired with the ASD Spectroradiometer (model) closely resemble those acquired from the hyperspectral imager (Section 4.3.2). The model shows notable distinctions when compared with a hyperspectral image, these include the loss of details, loss of shadows and changes in illumination (between pixels) are lost. This could be modeled in the future and incorporated in the multi-data dismount model if necessary. Also, the model dismisses imager effects and environment effects if the signatures are acquired with the ASD Spectroradiometer.

For the purposes of the study of dismount characterization and dismount detection, the model is of great advantage when compared to hyperspectral imager. The computer aided multi-data model allows rapid modification of scenes, change of signatures,

62

enhancement, dismissal or modification of environmental effects, replication of images, model reuse and more. The capability of creating a dismount model, where multi-data signatures are fused to the model and the ability of easy manipulation and development, considerably streamlines the research processes. The model also grows the potential of generating improvements on characterization of individuals by an efficient, easy to acquire, quick to develop, dismount modeling design. This comprehensive modeling capability provides the competence to explore hyperspectral imaging methods and exploit hyperspectral signatures unique characteristics for dismount detection and characterization endeavors.

5.2 Future Work

The goal of creating a platform for the study and modification of dismount models motivated our multi-data dismount system modeling. Despite the evidence of this success, there are still a variety of avenues in which details and enhancements to the model may be incorporated.

Certainly, a major area for study will be the modification of Spectroradiometer data (model's signatures) to copy that acquired with hyperspectral imagers. A sample data set of hyperspectral images are required to produce a model of a variety of imager specific noise effects, atmospheric and environmental conditions. These models will enhance the ability of the multi-data dismount model to reflect any atmospherics and distinctive imager specific requirements.

Bibliography

[1] *Environmental Health and Safety, Laser Fundamentals.* URL http://web.princeton.edu/sites/ehs/laserguide/index.htm.

[2] "Defense Advance Research Project Agency, Combat Zones that See", 2003.

[3] "United States Air Force Basic Doctrine, Air Force Doctrine Document 1", November 2003.

[4] *Modeling the Physiological Human, 3D Physiological Human Wokshop, 3DPH*, Lecture Notes in Computer Science. Springer, Germany, 2009. URL http://3dph.miralab.unige.ch/.

[5] Adams J., Smith M. "Spectral mixing modeling: A new analysis of rock and soil types at the Viking Lander I site." *J. Geophys. Res*, 91:8098–8112, 1986.

[6] Army Research Office, United States. "Efficient and Robust Algorithms for Real-time Video Tracking of Multiple Moving Targets", 2007. Proposed.

[7] Balan A., Black M. Davis J. Haussecker H., Sigal L. "Detailed Human Shape and Pose from Images". *IEEE Computer Vision and Pattern Recognition (CVPR)*, 2007.

[8] Ballard, D. "Generalizing the Hough transform to detect arbitrary shapes." *Pattern Recognition*, 13, 1981.

[9] Bhanu B., Chen H. *Advances in Pattern Recognition, Human Ear Recognition by Computer.* Springer.

[10] Bookstein, F. L. "Morphometric Tools for Landmark Data: Geometry and Biology." *Cambridge University Press*, 1991.

[11] Borengasser, M. "Hyperspectral remote sensing." *AccessScience, McGraw-Hill Companies*, 2003.

[12] Brooks, A. *Improved Multispectral Skin Detection and its application to search space reduction for dismount detection based on Histogram of Oriented Gradients.* Master's thesis, AFIT, October 2005.

[13] Canny, J. "A computational approach to edge detection." *IEEE Pattern Analysis and Machine Intelligence*, 8:679–714, 1986.

[14] Chuang J., Ko M., Tsai C. *Skeletonization of Three-Dimensional Object Using Generalized Potential Field.*, volume 22. IEEE Trans. PAMI, 2000.

[15] Clark, J.D. *Distributed Spacing Stochastic Feature Selection and its Application to Textile Classification.* Ph.D. thesis, AFIT, 2011.

[16] Climer, J. *Impact of Articulations in Pose and Aspect Angle on HOG features for a multispectral Dismount Detector System*. Master's thesis, AFIT, March 2011.

[17] Corporation, Space Computer. "Hyperspectral Imaging via LCTF, PHIRST Light II Operator Manual". March 2005.

[18] Dalal N., Cordelia S., Bill T. "Human Detection Using Oriented Histograms of Flow and Appearance". *Computer Vision*, 3952 of Lecture Notes in Computer Science:428–441, 2006.

[19] Dictionaries, Oxford. URL http://oxforddictionaries.com/.

[20] Fang Y., Ninomiya Y. Horn B.K.P. Masaki I., Yamada K. "A shape-independent method for pedestrian detection with far-infrared images". *IEEE*, Vehicular Technology:1679–1697, 2006.

[21] FieldSpec3. "ASD Inc". URL http://www.asdi.com/products/fieldspec-3.

[22] Gutierrez M., Vexo F. Moccozet L. Magnenat-Thalmann N. Mortara M. Spagnuolo M., Thalmann D. "An Ontology of Virtual Humans: incorporating semantics into human shapes". *Visual Computer*, 23(3):207–218, 2007.

[23] Hastie T., Friedman J., Tibshirani R. *The Elements of Statistical Learning, Data Mining, Interface and Prediction*. Springer Series in Statistics, second edition edition, 2009. ISBN 978038784857.

[24] Hilaga M., Kohmura T. Kunii T.L., Shinagawa Y. "Topology Matching for Fully Automatic Similarity Estimation of 3D Shapes." *Proc. of ACM SIGGRAPH*, 2001.

[25] Kendall, D.G. *The diffusion of shape, Advances in Applied Probability 9*. Kluwer Academic.

[26] Kerekes J., Baum J. "Hyperspectral Imaging System Modeling". *LINCOLN LABORATORY*, 14(1):117–129, 2003.

[27] Lindeberg, T. "Edge detection and ridge detection with automatic scale selection." *International Journal of Computer Vision*, 30(2):117–154, 1998.

[28] MacLeod, N. "Generalizing and Extending the Eigenshape Method of Shape Space Visualization and Analysis". *Paleobiology*, 1(25):107138, 1999.

[29] Maier, M.J. *Estimating Anthropometric marker locations from 3-D Ladar Point Clouds*. Master's thesis, AFIT, 2011.

[30] Mardia, K. "Shape in Images". *Pattern Recognition form classical to modern approaches*, 2002.

[31] Rohlf F. J., Slice D. *Extensions of the Procrustes method for the optimal superimposition of landmarks.*, volume 39. Systematic Zoology, 1990.

[32] Shashua A., Hayu G., Gdalyahu Y. "Pedestrian detection for driving assistance systems, single-frame classification and system level performance." *Intelligent Vehicles Symposium IEEE*, 1–6, 2004.

[33] Sherwood, L. *Human Physiology from cells to systems.* Pacific Grove, CA, 7 edition, 2010. ISBN 978-0495391845.

[34] Short, N.M. "Technical and Historical Perspectives of Remote Sensing". URL http://rst.gsfc.nasa.gov/Intro/Part2_24.html.

[35] SpecTIR, LLC. "HyperSpecTIR Operators Manual". November 2008.

[36] Rochester Istitute of Technology, Chester F. Carlson Center for Imaging Science. "The DIRSIG User's Manual. Digital Imaging and Remote Sensing Image Generation Model", 2007. URL http://dirsig.org/docs/manual/manual.html.

[37] Thomas, F. "Face detection and recognition.", August 2004. URL http://w3.ualg.pt/~ftomaz/fr/fr.php.

[38] Walker, J. *The ability of geometric morphometric methods to estimate a known covariance matrix.*, volume 49. Systematic Biology, 2000.

[39] Wang C., Yuen M., Chang T. "From laser-scanned data to feature human model: a system based fuzzy logic concept." *Computer Aided Design*, 2003.

[40] Zhang W., Bergholm F. "Multi-scale blur estimation and edge type classification for scene analysis." *International Journal of Computer Vision*, 24(3):219–250, 1997.

[41] Zuccarello, N. "http://nickzucc.blogspot.com/2008/05/new-head-topology.html". website.

REPORT DOCUMENTATION PAGE

The public reporting burden for this collection of information is estimated to average 1 hour per response, including the time for reviewing instructions, searching existing data sources, gathering and maintaining the data needed, and completing and reviewing the collection of information. Send comments regarding this burden estimate or any other aspect of the collection of information, including suggestions for reducing this burden to Department of Defense, Washington Headquarters Services, Directorate for Information Operations and Reports (0704-0188), 1215 Jefferson Davis Highway, Suite 1204, Arlington, VA 22202-4302. Respondents should be aware that notwithstanding any other provision of law, no person shall be subject to an penalty for failing to comply with a collection of information if it does not display a currently valid OMB control number.
PLEASE DO NOT RETURN YOUR FORM TO THE ABOVE ADDRESS.

1. REPORT DATE (DD-MM-YYYY) 22-03-2012	2. REPORT TYPE Master's Thesis	3. DATES COVERED (From – To) Aug 2010 - Mar 2012

4. TITLE AND SUBTITLE	5a. CONTRACT NUMBER
Computer Aided Multi-Data Fusion Dismount Modeling	5b. GRANT NUMBER
	5c. PROGRAM ELEMENT NUMBER

6. AUTHOR(S)	5d. PROJECT NUMBER
Morales, Juan L. Capt USAF	5e. TASK NUMBER
	5f. WORK UNIT NUMBER

7. PERFORMING ORGANIZATION NAMES(S) AND ADDRESS(S) Air Force Institute of Technology Graduate School of Engineering and Management (AFIT/EN) 2950 Hobson Street, Building 641 WPAFB OH 45433-7765	8. PERFORMING ORGANIZATION REPORT NUMBER AFIT/GE/ENG/12-29

9. SPONSORING/MONITORING AGENCY NAME(S) AND ADDRESS(ES) Air Force Research Laboratory Human Signatures Branch David R. Bowden, Electrical Engineer 2800 Q Street, Building 824 Wright Patterson, OH 45433 david.bowden@wpafb.af.mil (937) 255-4458	10. SPONSOR/MONITOR'S ACRONYM(S) 711 HPW/RHXBA
	11. SPONSOR/MONITOR'S REPORT NUMBER(S)

12. DISTRIBUTION/AVAILABILITY STATEMENT
Approved for Public Release; Distribution Unlimited

13. SUPPLEMENTARY NOTES
This material is declared a work of the U.S. Government and is not subject to copyright protection in the United States.

14. ABSTRACT

Recent research efforts strive to address the growing need for dismount surveillance, dismount tracking and characterization. Current work in this area utilizes hyperspectral and multispectral imaging systems to exploit spectral properties in order to detect areas of exposed skin and clothing characteristics. Because of the large bandwidth and high resolution, hyperspectral imaging systems pose great ability to characterize and detect dismounts. A multi-data dismount modeling system where the development and manipulation of dismount models is a necessity.

This thesis demonstrates a computer aided multi-data fused dismount model, which facilitates studies of dismount detection, characterization and identification. The system is created by fusing: pixel mapping, signature attachment, and pixel mixing algorithms.

The developed multi-data dismount model produces simulated hyperspectral images that closely represent an image collected by a hyperspectral imager. The dismount model can be modified to fit the researcher's needs. The multi-data model structure allows the employment of a database of signatures acquired from several sources. The model is flexible enough to allow further exploitation, enhancement and manipulation. The multi-data dismount model developed in this effort fulfills the need for a dismount modeling tool in a hyperspectral imaging environment.

15. SUBJECT TERMS
Dismount Modeling, Hyperspectral Signature Attachment

16. SECURITY CLASSIFICATION OF:			17. LIMITATION OF ABSTRACT	18. NUMBER OF PAGES	19a. NAME OF RESPONSIBLE PERSON Jeffrey D. Clark, Lt Col. USAF
REPORT U	ABSTRACT U	c. THIS PAGE U	UU	82	19b. TELEPHONE NUMBER (Include area code) (937) 255-3636 x 4614 jeffrey.clark@afit.edu